

Initiated Chemical Vapor Deposition of Fluoropolymer Coatings for the
Surface Modification of Complex Geometries

by

Malancha Gupta

M.S. Chemical Engineering
Massachusetts Institute of Technology, 2005

B.S. Chemical Engineering
The Cooper Union, 2002

Submitted to the Department of Chemical Engineering
in Partial Fulfillment of the Requirements for the Degree of

DOCTOR OF PHILOSOPHY IN CHEMICAL ENGINEERING
AT THE
MASSACHUSETTS INSTITUTE OF TECHNOLOGY

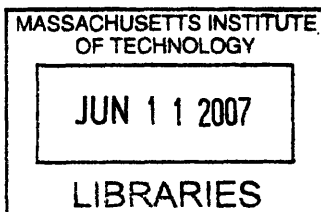
May 2007

© Massachusetts Institute of Technology, All Rights Reserved

Signature of Author:.....
Department of Chemical Engineering
May 17, 2007

Certified by:.....
Karen K. Gleason
Professor of Chemical Engineering
Thesis Supervisor

Accepted by:.....
William M. Deen
Professor of Chemical Engineering
Chair, Committee for Graduate Students



ARCHIVES

Initiated Chemical Vapor Deposition of Fluoropolymer Coatings for the Surface Modification of Complex Geometries

by

Malancha Gupta

Submitted to the Department of Chemical Engineering
on May 17, 2007 in Partial Fulfillment of the
Requirements for the Degree of
Doctor of Philosophy in Chemical Engineering

ABSTRACT

Initiated chemical vapor deposition (iCVD) is a one-step, solventless process that can be used to produce polymeric thin films. The iCVD technique has been used to polymerize a wide variety of vinyl monomers such as glycidyl methacrylate (adhesive) and 2-hydroxyethyl methacrylate (hydrophilic). The proposed polymerization mechanism is the classical free radical polymerization mechanism of vinyl monomers. Monomer and initiator gases are fed into a vacuum chamber where resistively heated wires are used to thermally decompose the initiator molecules into free radicals. The free radicals then attack the vinyl bonds of the monomer molecules. Propagation occurs on the surface of a cooled substrate.

This thesis presents an in-depth mechanistic study of the iCVD deposition of low surface energy poly(1H,1H,2H,2H-perfluorodecyl acrylate) (PPFDA) thin films. PPFDA films have many uses due to their hydrophobic and oleophobic properties. Fourier transform infrared spectroscopy and x-ray photoelectron spectroscopy of the iCVD PPFDA films showed complete retention of the fluorine moieties. Deposition rates as high as 375 nm/min were achieved. It was found that the deposition rate and molecular weight increases with decreasing substrate temperature and increasing monomer partial pressure. Quartz crystal microbalance measurements showed that these effects correlated with an increased monomer concentration at the surface. Dimensionless analysis was used to scale up this iCVD polymerization to a custom modified roll-to-roll reactor. The roll-to-roll process allows for the fast production of realistic size samples.

The use of liquid solvents in membrane coating processes often creates a blanket coating in which the pores are clogged due to surface tension problems and wettability. These problems do not exist for solventless processes such as iCVD. This thesis presents the use of the iCVD technique to functionalize electrospun fiber mats and polymeric capillary pore membranes in order to make water-repellant, self-cleaning membranes. X-ray photoelectron microscopy data confirmed the presence of the PPFDA coating on the topside and the backside of the membranes and electron microprobe analysis confirmed the presence of the coating along the pore wall. It was found that the iCVD process can be used to functionalize membranes with very high aspect ratio (~80:1) pores.

Thesis Supervisor: Karen K. Gleason
Title: Professor of Chemical Engineering

Acknowledgments

My MIT experience has had its bumps, but at least it was never boring! Anyway, it all worked out at the end and I would like to thank the people who helped me get to the finish line. First of all, I would like to thank my advisor Karen K. Gleason. She offered me a position in her lab and allowed me to grow as a researcher by letting me explore my own ideas. She gave me compliments when I needed it the most and I always felt that my work was appreciated. I would like to thank her for being a great advisor and a great mentor.

Next I would like to thank my family: my mom (Ujjayini Gupta), my dad (Seshadri Gupta), and my brother (Dr. Dr. Rajarsi Gupta, PhD, MD). They have always been there to listen to me and to help me. They have always had the highest expectations for me and this is the reason for my motivation. I would especially like to thank my mom for visiting me in Boston numerous times and for always being there when I need her.

I would also like to thank my close friends John Hennessy and Andrew (AJ) Allen. They have had to listen to me for hours on a daily basis and have provided me with several car rides. A special shout out to AJ who also helped me with the piping work for the roll-to-roll reactor. I would also like to thank my other friends at MIT: Smeet, Phuong, Corey, Hiroyo, Julie, Brad, Mark, Jodie.....

I would like to thank my thesis committee members Professor Jefferson Tester and Professor Herbert Sawin. I would like to thank the Gleason group especially Tyler Martin who brought me up to speed when I first joined. I would like to thank all the folks at the ISN who helped me with the roll-to-roll project and my two UROPS: Lara Kostun

and Natalie Pinkerton. I would also like to thank my collaborators at MIT Minglin Ma and Professor Gregory Rutledge and my collaborators at Dupont Dr. Yefim Brun and Dr. Vivek Kapur.

Table of Contents

Title Page	1
Abstract	2
Acknowledgments	3
Table of Contents	5
List of Figures	7
List of Tables	11
Chapter 1: Introduction	12
1.1 Initiated Chemical Vapor Deposition (iCVD)	13
1.2 Low Surface Energy Fluoropolymer Coatings	16
1.3 Scale-Up.....	19
1.4 Surface Modification of Complex Geometries	22
1.5 Scope of Thesis	24
1.6 References.....	25
Chapter 2:Initiated Chemical Vapor Deposition (iCVD) of Poly(1H,1H,2H,2H-Perfluorodecyl Acrylate) (PPFDA) Thin Films	27
2.1 Abstract.....	28
2.2 Introduction.....	29
2.3 Experimental Methods.....	31
2.4 Results and Discussion	33
2.4.1 Material Characterization	33
2.4.2 Effect of Substrate Temperature	39
2.4.3 Effect of Monomer Partial Pressure.....	41
2.4.4 Kinetics	44
2.5 Conclusion	45
2.6 Acknowledgment	46
2.7 References.....	47
Chapter 3:Large Scale Initiated Chemical Vapor Deposition of Poly(glycidyl methacrylate) Thin Films	49
3.1 Abstract.....	50
3.2 Introduction.....	51
3.3 Experimental Methods.....	53
3.4 Results and Discussion	56
3.4.1 Dimensionless Analysis.....	56
3.4.2 Large Area Deposition.....	58
3.4.3 Moving Substrate	63
3.5 Conclusion	66
3.6 Acknowledgment	67
3.7 References.....	68

Chapter 4: Surface Modification of High Aspect Ratio Pores and Surface Features by initiated Chemical Vapor Deposition (iCVD)	70
4.1 Abstract.....	71
4.2 Introduction.....	72
4.3 Experimental Methods.....	75
4.4 Results and Discussion	76
4.5 Conclusion	86
4.6 Acknowledgment	87
4.7 References.....	88
Chapter 5: Surface Modification of High Aspect Ratio Pores and Surface Features by initiated Chemical Vapor Deposition (iCVD)	90
5.1 Abstract.....	91
5.2 Introduction.....	92
5.3 Experimental Methods.....	96
5.4 Results and Discussion	97
5.4.1 PPFEMA-coated Beaded and Non-Beaded PCL Fiber Mats	97
5.4.2 PPFEMA-coated PMMA Porous Fiber Mats	101
5.5 Conclusion	103
5.6 Acknowledgment	104
5.7 References.....	105
Chapter 6: Conclusions and Future Work	107
6.1 Conclusions.....	108
6.1.1 Initiated Chemical Vapor Deposition of PPFDA Thin Films.....	108
6.1.2 Large Scale Initiated Chemical Vapor Deposition	109
6.1.3 Surface Modification of High Aspect Ratio Pores	109
6.1.4 Surface Modification of Electrospun Mats.....	110
6.2 Future Work.....	110

List of Figures

Chaper One

Figure 1-1: Picture of batch reactor. Monomer and initiator (tert-butyl peroxide) gases continuously flow into the reactor. The polymerization mechanism is the classical free radical polymerization. p.14

Figure 1-2: a) Glycidyl methacrylate (GMA) and b) 2-hydroxyethyl methacrylate (HEMA) are two types of monomers that have been polymerized using the initiated chemical vapor deposition process (iCVD). Poly(glycidyl methacrylate) films can be patterned into small features using e-beam lithography and poly(2-hydroxyethyl methacrylate) films are hydrophilic and therefore can be used as hydrogels. p.15

Figure 1-3: FTIR spectra of poly(glycidyl methacrylate) films created using a) iCVD, b) plasma CVD, and c) conventional polymerization. The epoxide functionality has characteristic absorption peaks at wavenumbers of 907, 848, and 760 cm^{-1} . p.16

Figure 1-4: There are several examples of superhydrophobic, self-cleaning materials that can be found in Nature such as the a) lotus leaf, b) insect wings, and c) legs of a water strider. These naturally occurring materials achieve their superhydrophobicity through a combination of low surface energy chemistry and roughness. p.18

Figure 1-5: a) The configuration of the chiller and the filament array in the small-scale reactor. b) In order to scale-up the process, a chiller and filament array needed to be added to the roll-to-roll chamber. p.21

Figure 1-6: The inside of the custom-modified plasma roll-to-roll reactor. p.22

Figure 1-7: There are several applications for the surface modification of pores and trenches. p.23

Chaper Two

Figure 2-1: FTIR spectra of the iCVD PPFDA film samples in the TS series (top) and liquid PFDA monomer (bottom) in a) the region between 1900 cm^{-1} and 900 cm^{-1} and b) the region between 3150 cm^{-1} and 2800 cm^{-1} . The dashed lines represent the location of the CF_2 and CF_3 groups and the asterisks in both monomer spectra represent the location of the C=C bond. The C=O peak at 1741 cm^{-1} was used to normalize the intensity of the TS4 spectrum. The intensities of the other spectra reflect the different thicknesses of the films. p.35

Figure 2-2: XPS spectra of the iCVD PPFDA film sample TS1. a) Survey scan showing the atomic concentration of fluorine, oxygen, and carbon in the polymer film. b) High resolution scan of the C 1s peak with seven resolved peaks. p.36

Figure 2-3: Deposition rate as a function of the substrate temperature plotted in an Arrhenius form where the solid line represents the results of a linear regression to the data. (Series TS, Table 2-1) p.40

Figure 2-4: Deposition rate (circles) as a function of monomer partial pressure at a constant substrate temperature of 44°C. (Series PM, Table 2-1) The squares represent the predicted values of the kinetic model. p.42

Figure 2-5: QCM measurements of the monomer adsorption as a function of monomer partial pressure at a constant crystal temperature of 44°C. The solid line represents the regression to the BET isotherm. p.43

Figure 2-6: Details of the reaction steps that take place on the substrate surface during iCVD polymerization where I is the initiator and M is the monomer. p.44

Chaper Three

Figure 3-1: (a) Chemical structures of the tert-butyl peroxide initiator and the glycidyl methacrylate monomer. (b) Details of the polymerization mechanism where I is the initiator molecule and M is the monomer. p.51

Figure 3-2: Schematic of the custom modified iCVD roll-to-roll system. p.54

Figure 3-3: Substrate temperature (T_s) as a function of the heat exchanger setting (T_c) and filament temperature (T_f). p.55

Figure 3-4: Deposition rate as a function of the filament temperature plotted in an Arrhenius form. The substrate temperature is held constant at 35 °C. p.60

Figure 3-5: Deposition rate as a function of the substrate temperature plotted in an Arrhenius form. The filament temperature is held constant at 245 °C. p.61

Figure 3-6: Number-average molecular weight, M_n , as a function of substrate temperature plotted in an Arrhenius form. The filament temperature is held constant at 245 °C. p.62

Figure 3-7: FTIR spectra of PGMA films deposited at various filament and substrate temperatures and the FTIR spectrum of conventionally polymerized PGMA. The epoxide group has absorption bands at 907, 848, and 760 cm^{-1} . p.63

Figure 3-8: Thickness uniformity of PGMA films deposited at a filament temperature of 245° and a substrate temperature of 35° for 10 minutes. (a) Placement of wafers along the cooling stage. (b) Plot showing thickness uniformity along both the x- and y-directions. p.65

Figure 3-9: Thickness as a function of the inverse of the substrate velocity. The solid squares represent the data for the moving substrate and the dashed line represents the data for the stationary substrate. p.66

Chapter Four

Figure 4-1: a) Topdown and b) cross section SEM micrographs of a 240 μm thick capillary pore membrane. The average pore diameter is 3 μm and the nominal porosity is 50%. c) Enlarged image of a membrane with a nominal porosity of 30%. p.74

Figure 4-2: a) Measured static contact angles for uncoated and coated membranes (topside and backside). b) Comparison of the experimental contact angles for uncoated (circles) and coated membranes (squares) and the contact angles predicted using the Cassie-Baxter model (triangles). The Cassie-Baxter model predicts the correct trend but underestimates the experimental values. p.79

Figure 4-3: Advancing and receding contact angle measurements for 50% porous membranes with pore lengths of 120 microns (unfilled) and 240 microns (filled). The measurements were taken from the topside (triangles) and the bottom side (squares). The low hysteresis measured on both sides confirms that coating has been achieved along the entire length of the inner pore wall. p.80

Figure 4-4: XPS survey scans for detection of the atomic concentration of fluorine, oxygen, and carbon in a) the uncoated membrane, b) the topside of the coated membrane, and c) the backside of the coated membrane. p.81

Figure 4-5. Electron microprobe data for membranes coated for 2 minutes (unfilled) and 5 minutes (filled). Three different membranes were employed: 30% porosity and 120 μm length (squares), 30% porosity and 240 μm length (circles), and 50% porosity and 240 μm length (diamonds). The average pore diameter for all the membranes was 3 μm . p.84

Figure 4-6: a) SEM cross-sectional micrograph of a silicon trench (3 μm width, 6 μm depth) conformally coated by a 0.25 μm thick layer of iCVD PPFDA. b) Enlarged image of the right side of the trench. c) A silicon trench (1 μm width, 6 μm depth) completely filled with a thick layer of iCVD PPFDA. p.86

Chapter Five

Figure 5-1: a) Contact angles on flat substrates can be estimated using Young's equation. Contact angles on rough surfaces can exist in one of two states b) the Wenzel state and c) the Cassie-Baxter state. In the Wenzel state, the water falls into the pores and there is high hysteresis. In the Cassie-Baxter state, the water sits on top of the pores and there is low hysteresis. p.95

Figure 5-2: SEM micrographs of a beaded PCL electrospun fiber mat a) before and b) after coating. There is no noticeable change in morphology after coating. p.97

Figure 5-3: XPS survey scans for detection of the atomic concentration of fluorine, oxygen, and carbon in a) an uncoated PCL mat and b) a PPFEMA coated PCL mat. p.98

Figure 5-4: Contact angles on the PCL electrospun fiber mats a) before and b) after coating. The contact angles increase after coating. p.100

Figure 5-5: Threshold sliding contact angles on the PPFEMA coated PCL electrospun fiber mats. p.101

Figure 5-6: SEM micrographs of the porous PMMA electrospun mats a) before and b) after coating. There is no noticeable change in morphology after coating. The nanopores remain open even after coating. p.102

Chapter Six

Figure 6-1: Comparison of two trenches coated with PGMA under reactor conditions in which all variables are kept the same except for the total reactor pressure. a) Trench coated at a reactor pressure of 370 mTorr ($P_m/P_{sat}=0.55$). b) Trench coated at a reactor pressure of 450 mTorr ($P_m/P_{sat}=0.67$). p.114

Figure 6-2: Comparison of two trenches coated with PGMA under reactor conditions in which all variables are kept the same except for the initiator flow rate. a) Trench coated at an initiator flow rate of 1 sccm ($P_m/P_{sat}=0.55$). b) Trench coated at an initiator flow rate of 3 sccm ($P_m/P_{sat}=0.37$). p.115

Figure 6-3: Trench coated with PPFDA (sample F). p.116

List of Tables

Chaper Two

Table 2-1: Process Conditions and Resultant Growth Rates for the iCVD PPFDA	p.32
Table 2-2: Atomic Percentages from XPS Survey Scan	p.38
Table 2-3: Atomic Percentages of Carbon Environments from C 1s XPS Spectra	p.38
Table 2-4: Weight Average Molecular Weight From GPC Measurements	p.39
Table 2-5: Comparison of iCVD rate constants for butyl acrylate and PFDA	p.45

Chapter Three

Table 3-1: List of reactor conditions and transport properties for the polymerization of glycidyl methacrylate in both the small-scale reactor and the roll-to-roll reactor.	p.58
--	------

Chaper Four

Table 4-1. Weight Gain and Calculated Thickness After 5 and 10 Minutes of iCVD PPFDA Coating	p.82
--	------

Chaper Six

Table 6-1: Process Conditions for Trench Coatings	p.113
---	-------

Chaper One:

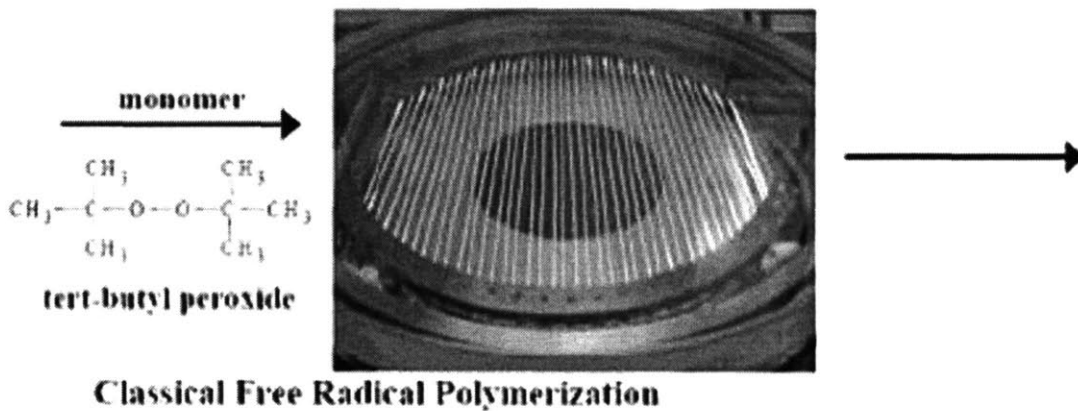
Introduction

1.1 Initiated Chemical Vapor Deposition (iCVD)

Initiated chemical vapor deposition (iCVD) is a low energy vapor deposition process (0.01 W/cm^2) that can be used to produce polymeric thin films in which the pendant chemical moieties are kept intact.¹ This all-dry process has environmental benefits because no solvents are used and this process can be used to conformally coat complex geometries² since the surface tension problems associated with liquids are not present. The proposed polymerization mechanism is the classical free radical polymerization mechanism of vinyl monomers. Monomer and initiator gases are fed into a vacuum chamber where resistively heated wires are used to thermally decompose the initiator molecules into free radicals. The free radicals diffuse to the substrate and adsorb onto the surface. The substrate temperature is kept cool to promote the adsorption of the free radicals as well as the monomer molecules. Initiation, propagation, and termination events occur on the surface of the cooled substrate to form a polymer film. (See Figure 1-1) iCVD has been used to polymerize a wide variety of vinyl monomers such as glycidyl methacrylate³ and 2-hydroxyethyl methacrylate.⁴ (See Figure 1-2) Tert-butyl peroxide is usually used as the initiator.

Other types of solvent-free polymerization processes such as continuous plasma polymerization and pulsed plasma polymerization require much higher energy inputs and the chemical functionalities of the monomer are often destroyed.^{5,6} (See Figure 1-3) The highest deposition rates achieved with pulsed plasma polymerization are typically on the order of 10 nm/min which is significantly lower than the deposition rates achieved using the iCVD process (up to 375 nm/min).⁵ The slow deposition rates found in plasma

polymerization are due to the complexity of the plasma process. The high energy of the plasma partially breaks apart the monomer, reducing the concentration available for polymerization. In contrast, the iCVD process only breaks the initiator and leaves the monomer completely intact. Additionally, there is a competition between etching and deposition in plasma processes⁷ where the iCVD process involves only deposition and does not involve etching.



Initiation:



Propagation:



Termination:

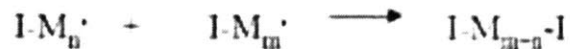
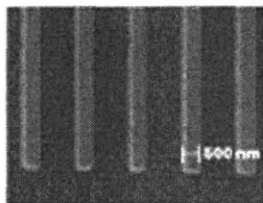
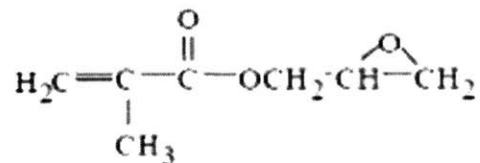


Figure 1-1: Picture of iCVD reactor. Monomer and initiator (usually tert-butyl peroxide) gases continuously flow into the reactor. The polymerization mechanism is a classical free radical polymerization.

a)

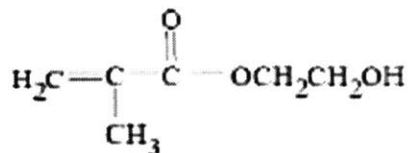
glycidyl methacrylate (GMA)



Y. Mao and K.K. Gleason. *Langmuir*, 2004.

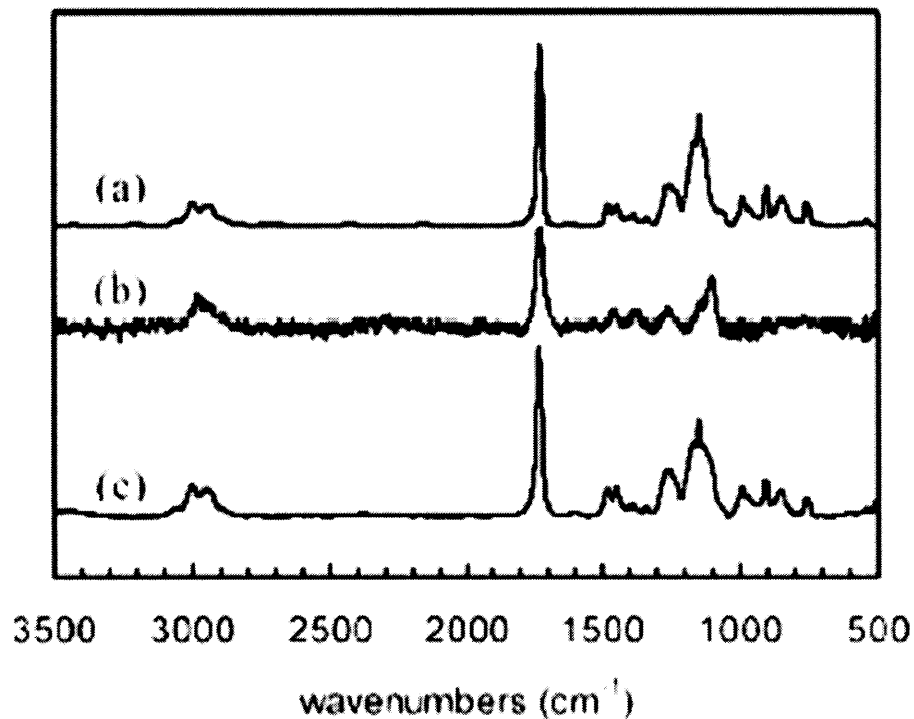
b)

2-hydroxyethyl methacrylate (HEMA)



K. Chan and K.K. Gleason. *Langmuir*, 2005.

Figure 1-2: a) Glycidyl methacrylate (GMA) and b) 2-hydroxyethyl methacrylate (HEMA) are two types of monomers that have been polymerized using the iCVD process. Poly(glycidyl methacrylate) films can be patterned into small features using e-beam lithography and poly(2-hydroxyethyl methacrylate) films are hydrophilic and therefore can be used as hydrogels.



Y. Mao and K.K. Gleason, *Langmuir*, 2004.

Figure 1-3: FTIR spectra of poly(glycidyl methacrylate) films created using a) iCVD, b) plasma CVD, and c) conventional polymerization. The epoxide functionality has characteristic absorption peaks at wavenumbers of 907, 848, and 760 cm^{-1} . It can be seen that the iCVD process keeps the epoxide functionality intact.

1.2 Low Surface Energy Fluoropolymer Coatings

Low surface energy polymeric coatings have many uses due to their hydrophobic and oleophobic properties.^{8,9} For example, fluorinated polymer coatings have been used to modify various surfaces such as carbon nanotubes² and textiles.^{10,11} Polymers containing CF_3 end groups have a lower surface energy (9.3 mN/m) than poly(tetrafluoroethylene) (PTFE, 18 mN/m)¹² and therefore it is advantageous to create low surface energy coatings from acrylate and methacrylate monomers that contain CF_3 end groups.¹³

The hydrophobicity of a flat substrate can be increased by either lowering the surface energy through a change in surface chemistry or by adding roughness to the surface.^{14,15} It has been found that the maximum contact angle that can be achieved on a flat surface using surface chemistry alone is 120° ¹⁶ and static contact angles higher than 120° can only be achieved through the addition of surface roughness. There are several examples of naturally occurring superhydrophobic, self-cleaning materials that can be found in Nature. (See Figure 1-4) These natural materials achieve their superhydrophobicity through a combination of low surface energy chemistry and roughness.

A rough, hydrophobic surface can exist in two different states: Wenzel or Cassie-Baxter. In the Wenzel state,¹⁷ the water droplet penetrates the pore and there is a large hysteresis between advancing and receding contact angles. In the Cassie-Baxter state,¹⁸ the water droplet does not penetrate the pore and instead sits on top of the pores. There is low hysteresis in the Cassie-Baxter state. For practical applications that require hydrophobicity, water droplets should not penetrate the pores and therefore the Cassie-Baxter state is required. In the Cassie-Baxter model, the apparent contact angle, θ^* , is $\cos \theta^* = \phi_s \cos \theta - \phi_v$, where θ is the contact angle on a flat surface and ϕ_s and ϕ_v are the solid-liquid and air-liquid contact area per unit projected surface area respectively.

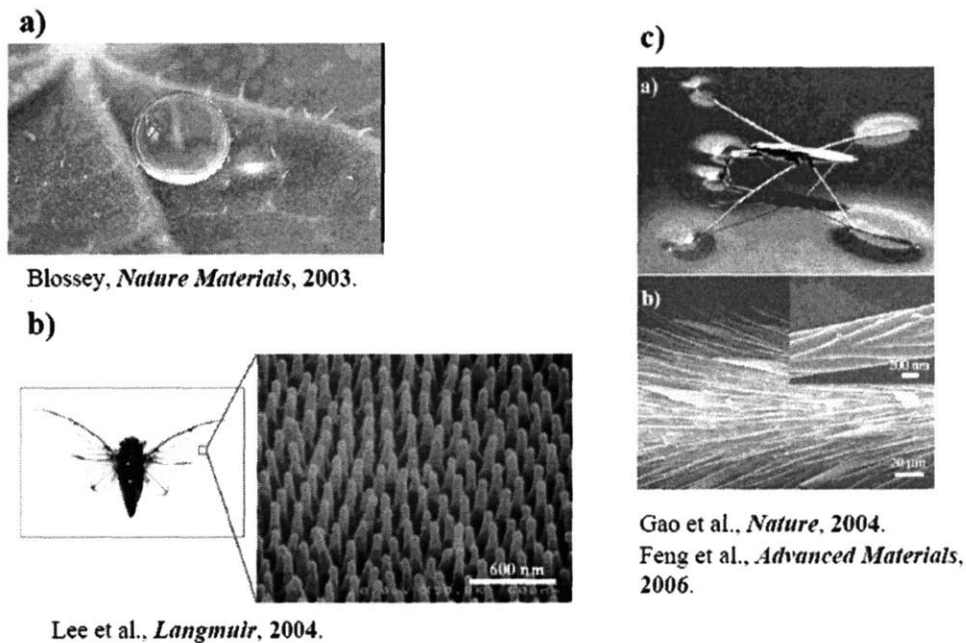


Figure 1-4: There are several examples of superhydrophobic, self-cleaning materials that can be found in Nature such as a) the lotus leaf, b) insect wings, and c) the legs of a water strider. These naturally occurring materials achieve their superhydrophobicity through a combination of low surface energy chemistry and roughness.

The goal of this thesis is to use the iCVD technique to create low surface energy fluoropolymer coatings. We will study the iCVD polymerization of perfluoroalkylethyl methacrylate (PFEMA, $\text{CH}_2=\text{C}(\text{CH}_3)\text{COOCH}_2\text{CH}_2(\text{CF}_2)_n\text{CF}_3$ where $n=5-13$, $n_{\text{avg}}=8$) and 1H,1H,2H,2H-perfluorodecyl acrylate (PFDA, $\text{CH}_2=\text{CHCOOCH}_2\text{CH}_2(\text{CF}_2)_7\text{CF}_3$). Understanding the mechanistic aspects of the iCVD polymerization of fluorinated monomers will aid the optimization of the process. We will use this iCVD process to modify rough surfaces with fluoropolymer coatings in order to create superhydrophobic surfaces like those found in Nature.

1.3 Scale-Up

There has been significant work in scaling up inorganic vapor deposition processes. Large area deposition of amorphous silicon has been studied in a plasma roll-to-roll reactor^{19, 20}, a plasma in-line deposition system²¹, and a large area hot wire CVD apparatus²². An in-line deposition system has also been used to create films containing copper, indium, gallium, and selenium²³. The pulsed laser deposition of tantalum pentoxide films has been scaled up to larger areas through the use of a rotating substrate.²⁴

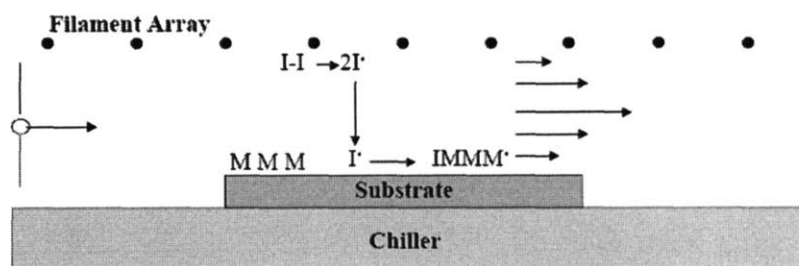
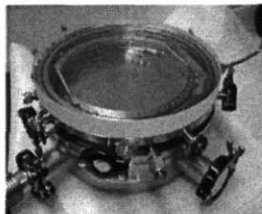
Currently all iCVD polymerizations have been conducted in small-scale reactors (diameters less than 300 mm) in which the substrate remains stationary and the deposition occurs between pump down and pump up periods. Another goal of this thesis is to scale-up the iCVD process to a roll-to-roll reactor in which the uncoated substrate continuously enters the reaction zone at a steady rate and exits as coated. The roll-to-roll process allows for the production of realistic size samples that can be easily tested for various applications. The roll-to-roll process also saves the time it takes to load the substrate, pump down to the reaction pressure, heat the filament, and pump back up. For example, the small-scale iCVD polymerization processes take approximately 30 minutes to load the sample and pump down and 30 minutes to unload the sample and shutdown. The actual deposition takes only a few minutes.

The small-scale iCVD reactors are custom-built. The reaction chamber is cylindrical with a diameter of 240 mm and a height of 33 mm. The roll-to-roll reactor has a 0.16 m³ chamber that contains one unwinder roll, three spreader rolls to prevent wrinkling of the web, one tension roll, and one rewinder roll (PLASMAtech model V-

160GK-RT). The maximum length of the roll is 30 cm and the maximum diameter of the roll is 16 cm. In order to scale-up the iCVD process, a chiller and filament array need to be added to the roll-to-roll chamber and the chamber needs to be modified in order to reproduce the same gas flow profiles and filament to substrate standoff as the smaller-scale iCVD reactors. (See Figure 1-5) Figure 1-6 shows the inside of the custom-modified roll-to-roll chamber. A vertical 35 cm by 43 cm stainless steel baffled heat exchanger is placed between the filament array and the rolls. The heat exchanger serves to cool the substrate and to physically force the inlet gases to flow along the direction of the substrate and exit uniformly. The width of the heat exchanger spans the entire depth of the reaction chamber. The monomer and initiator gases are uniformly distributed across the entire width of the substrate using a distributor tube that is 30 cm long and 1.3 cm in diameter and contains ten 1 millimeter holes. A square filament array holder was custom designed to be wider (35 cm) than the roll width (30 cm) in order to ensure that the edges of the roll will get exposure to the filaments and will therefore have the same thickness as the rest of the substrate. The filaments are strung across the width of the substrate in order to achieve uniformity across the width of the substrate, perpendicular to the direction of gas flow. As the substrate moves along, its entire width will be exposed to each separate filament.

The goal of this thesis is to scale-up the iCVD process to a roll-to-roll reactor using dimensionless analysis. Dimensionless analysis ensures that convection and diffusion have the same contribution in both the small-scale reactor and the roll-to-roll reactor.

a)



b)

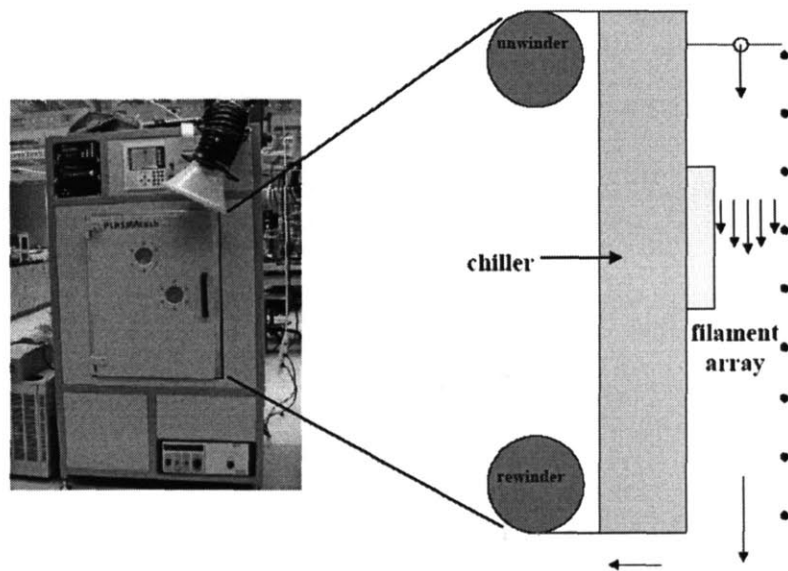


Figure 1-5: a) The configuration of the chiller and the filament array in the small-scale iCVD reactor. b) In order to scale-up the process, a chiller and filament array need to be added to the roll-to-roll chamber.

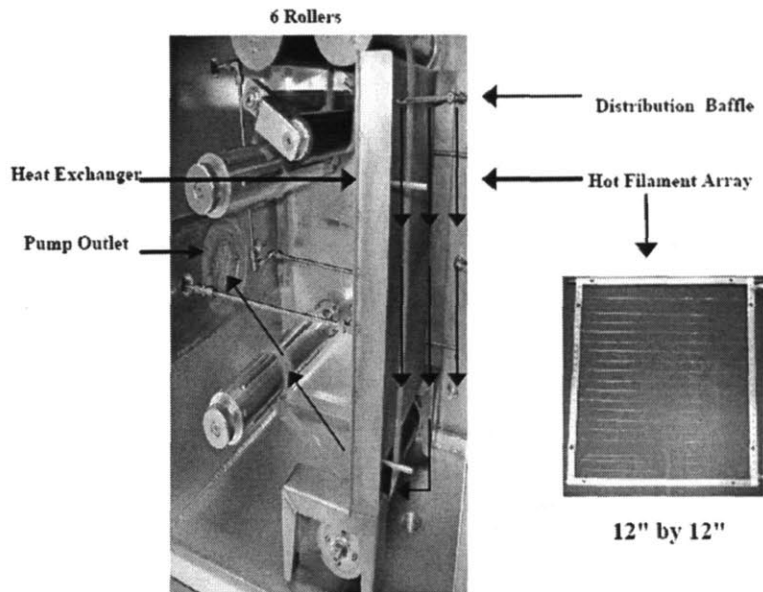
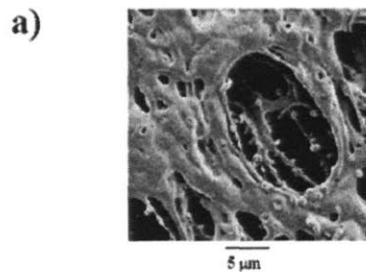


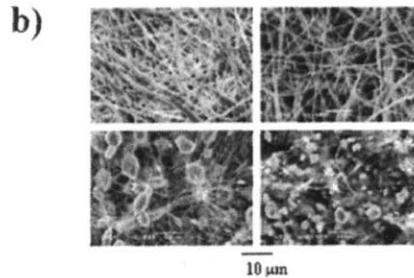
Figure 1-6: The inside of the custom-modified iCVD roll-to-roll reactor.

1.4 Surface Modification of Complex Geometries

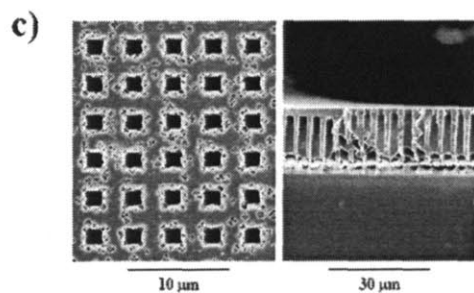
The surface modification of high aspect ratio microstructures has applications in several fields such as biology, textiles, and microelectronics. Silicon membranes have been functionalized with biotin in order to create membranes that can selectively capture biological organisms.²⁵ Atomic layer deposition has been used to conformally coat silicon trenches for microelectronic applications.²⁶ Plasma polymerization has been used to coat silicon trenches to make non-adhesive silicon molds for soft lithography.²⁷ Plasma-induced grafting has been used to attach hydrophilic polymers onto the surfaces of hydrophobic membranes in order to prevent membrane fouling caused by protein adsorption.^{28,29} (See Figure 1-7)



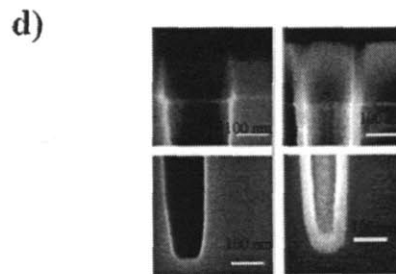
Hydrophilic Millipore Filters
Wavhal et al. *Journal of Membrane Science*, 2002



Hydrophobic Electrospun Fiber Mats
Ma et al., *Macromolecules*, 2005



Biotin-Functionalized Silicon Membranes
Letant et al. *Nature Materials*, 2003



Dielectric for Integrated Circuit
Hausmann et al. *Chemistry of Materials*, 2002

Figure 1-7: The surface modification of high aspect ratio microstructures has applications in several fields.

The goal of this thesis is to use the iCVD technique to functionalize the surfaces of complex 3-dimensional objects. We will use the iCVD process to apply poly(perfluoroalkylethyl methacrylate) and poly(1H,1H,2H,2H-perfluorodecyl acrylate) coatings onto various structures such as electrospun mats, capillary pore membranes, and silicon trenches.

1.5 Scope of Thesis

Chapter 2 is an in-depth mechanistic study of the iCVD polymerization of 1H,1H,2H,2H-perfluorodecyl acrylate (PFDA) which encompasses the chemical structure of the deposited film, the adsorption isotherm of the monomer species, and the deposition kinetics of the iCVD fluoropolymer film.

Chapter 3 focuses on the scale up of the iCVD polymerization of glycidyl methacrylate. Since the iCVD polymerization of different vinyl monomers all use similar parameters, this scale up can be applied to the scale up of other vinyl monomers.

Chapter 4 shows how the iCVD technique can be used to functionalize capillary pore membranes with PPFDA in order to make water-repellant, self-cleaning membranes. The capillary pore membranes used in this study have cylindrical pores of well-defined diameter which form ordered arrays. The capillary pore membrane geometry can be systematically varied (pore diameter, pore length, and degree of porosity), enabling fundamental examination of the iCVD process for coating features with different aspect ratios (ratio between length and diameter). This work was done in collaboration with the DuPont-MIT Alliance.

Chapter 5 shows how the iCVD technique can be combined with the electrospinning technique to create superhydrophobic fiber mats. This work was done in collaboration with Professor Rutledge's group at MIT.

1.6 References

- (1) Mao, Y.; Gleason, K. K. *Langmuir* **2006**, *22*, 1795-1799.
- (2) Lau, K. K. S.; Bico, J.; Teo, K. B. K.; Chhowalla, M.; Amaratunga, G. A. J.; Milne, W. I.; McKinley, G. H.; Gleason, K. K. *Nano Lett.* **2003**, *3*, 1701-1705.
- (3) Mao, Y.; Gleason, K. K. *Langmuir* **2004**, *20*, 2484-2488.
- (4) Chan, K.; Gleason, K. K. *Langmuir* **2005**, *21*, 8930-8939.
- (5) Coulson, S. R.; Woodward, I.; Badyal, J. P. S.; Brewer, S. A.; Willis, C. *Chem. Mater.* **2000**, *12*, 2031-2038.
- (6) Coulson, S. R.; Woodward, I.; Badyal, J. P. S.; Brewer, S. A.; Willis, C. *Langmuir* **2000**, *16*, 6287-6293.
- (7) d'Agostino, R. *Plasma Deposition, Treatment, and Etching of Polymers*; Academic Press: Boston, 1990.
- (8) Feng, L.; Li, S.; Li, Y.; Li, H.; Zhang, L.; Zhai, J.; Song, Y.; Liu, B.; Jiang, L.; Zhu, D. *Adv. Mater.* **2002**, *14*, 1857-1860.
- (9) Chen, W.; Fadeev, A. Y.; Hsieh, M. C.; Oner, D.; Youngblood, J.; McCarthy, T. J. *Langmuir* **1999**, *15*, 3395-3399.
- (10) Furukawa, Y.; Kotera, M. *J. Appl. Polym. Sci.* **2003**, *87*, 1085-1091.
- (11) McCord, M. G.; Hwang, Y. J.; Qiu, Y.; Hughes, L. K.; Bourham, M. A. *J. Appl. Polym. Sci.* **2003**, *88*, 2038-2047.
- (12) Thunemann, A. F.; Lieske, A.; Paulke, B.-R. *Adv. Mater.* **1999**, *11*, 321-324.
- (13) Park, I. J.; Lee, S. B.; Choi, C. K.; Kim, K. J. *J. Colloid Interface Sci.* **1996**, *181*, 284-288.
- (14) X. Feng, L. Jiang, *Adv. Mater.* **2006**, *18*, 3063.
- (15) H. Chen, F. Zhang, S. Fu, X. Duan, *Adv. Mater.* **2006**, *18*, 3089.
- (16) A. Lafuma, D. Quere, *Nat. Mater.* **2003**, *2*, 457.
- (17) R. N. Wenzel, *Ind. Eng. Chem.* **1936**, *28*, 988.
- (18) A. B. D. Cassie, S. Baxter, *Trans. Faraday Soc.* **1944**, *40*, 546.
- (19) M. Izu, S. Ovshinsky, *Thin Solid Films* **1984**, *119*, 55.

-
- (20) R.E.I. Schropp and M. Zeman, *IEEE Trans. Electron Dev.* **1999**, *46*, 2086.
- (21) J. Rudiger, H. Brechtel, A. Kottwitz, J. Kuske, U. Stephan, *Thin Solid Films* **2003**, *427*, 16.
- (22) A. Ledermann, U. Weber, C. Mukherjee, B. Schroeder, *Thin Solid Films* **2001**, *395*, 61.
- (23) G. Voorwinden, R. Kniese, M. Powalla, *Thin Solid Films* **2003**, *431-432*, 538.
- (24) S. Boughaba, G.I. Sproule, J.P. McCaffrey, M. Islam, M.J. Graham, *Thin Solid Films* **358** (2000) 104.
- (25) S. E. Létant, B. R. Hart, A. W. Van Buuren, L. J. Terminello, *Nat. Mater.* **2003**, *2*, 391.
- (26) R. G. Gordon, D. Hausmann, E. Kim, J. Shepard, *Chem. Vap. Deposition* **2003**, *9*, 73.
- (27) L. P. Yeo, Y. H. Yan, Y. C. Lam, M. B. Chan-Park, *Langmuir* **2006**, *22*, 10196.
- (28) D. S. Wavhal, E. R. Fisher, *Journal of Membrane Science* **2002**, *209*, 255.
- (29) H.-Y. Yu, M.-X. Hu, Z.-K. Xu, *Plasma Process. Polym.* **2005**, *2*, 627.

Chapter Two:
Initiated Chemical Vapor Deposition (iCVD) of
Poly(1H,1H,2H,2H-Perfluorodecyl Acrylate)
(PPFDA) Thin Films

Published in Langmuir:

Malancha Gupta and Karen K. Gleason. "Mechanistic Study of the Initiated Chemical Vapor Deposition (iCVD) of Poly(1H,1H,2H,2H-Perfluorodecyl Acrylate) (PPFDA) Thin Films", *Langmuir*, 22, 10047-10052, 2006.

2.1 Abstract

A solvent-free initiated chemical vapor deposition (iCVD) process was used to create low surface energy poly(1H,1H,2H,2H-perfluorodecyl acrylate) (PPFDA) thin films at deposition rates as high as 375 nm/min. Fourier transform infrared spectroscopy (FTIR) and x-ray photoelectron spectroscopy showed full retention of the fluorine moieties and no measurable crosslinking was detected. Additionally the FTIR studies support the hypothesis that film deposition results from vinyl polymerization. For all iCVD PPFDA films, the static contact angle was found to be $120.8^\circ \pm 1.2^\circ$. The roughness of the films was found to be between 14.9 nm and 19.8 nm RMS and the refractive index of the films was found to be between 1.36 and 1.37. The deposition rate was studied as a function of the substrate temperature and the partial pressure of the monomer. It was found that the deposition rate increases with decreasing substrate temperature and increasing monomer partial pressure. It was also found that the molecular weight increases with decreasing substrate temperature and increases with increasing monomer partial pressure. The highest molecular weight measured was 177300 with a polydispersity of 2.27. Quartz crystal microbalance (QCM) measurements showed that these effects correlated with an increased monomer concentration at the surface. The deposition rate data and the QCM data were quantitatively analyzed to find the rate constants of the process using a previously published model for the iCVD process involving nonfluorinated monomers. The determined values of the rate constants of the surface polymerization were found to be similar to the rate constants measured in liquid phase free radical polymerization. The kinetic data found in this paper can now be used to study iCVD deposition onto substrates with more complex geometries.

2.2 Introduction

Initiated chemical vapor deposition (iCVD) is a low energy vapor deposition process (0.01 W/cm^2) that can be used to produce polymeric thin films in which the pendant chemical moieties are kept intact.¹ This all-dry process has environmental benefits because no solvents are used and this process can be used to conformally coat complex geometries² since the surface tension problems associated with liquids are not present. iCVD has been used to polymerize a wide variety of vinyl monomers such as glycidyl methacrylate³ and 2-hydroxyethyl methacrylate.⁴ Tert-butyl peroxide is used as the initiator. The proposed polymerization mechanism is the classical free radical polymerization mechanism of vinyl monomers. Monomer and initiator gases are fed into a vacuum chamber where resistively heated wires are used to thermally decompose the initiator molecules into free radicals. The free radicals diffuse to the substrate and adsorb onto the surface. The substrate temperature is kept cool to promote the adsorption of the free radicals as well as the monomer molecules. Initiation, propagation, and termination events occur on the surface of the cooled substrate to form a polymer film.

Low surface energy polymeric coatings have many uses due to their hydrophobic and oleophobic properties.^{5,6} For example, fluorinated polymer coatings have been used to modify various surfaces such as carbon nanotubes² and textiles.^{7,8} Polymers containing CF_3 end groups have a lower surface energy (9.3 mN/m) than poly(tetrafluoroethylene) (PTFE, 18 mN/m)⁹ and therefore it is advantageous to create low surface energy coatings from acrylate and methacrylate monomers that contain CF_3 end groups.¹⁰

The iCVD technique has recently been used to polymerize perfluoroalkylethyl methacrylate ($\text{CH}_2=\text{C}(\text{CH}_3)\text{COOCH}_2\text{CH}_2(\text{CF}_2)_n\text{CF}_3$ where $n=5-13$) in order to create low

surface energy copolymer films¹¹ and superhydrophobic mats.¹² These superhydrophobic mats were created by using the iCVD process to coat electrospun fiber mats. Scanning electron microscope images and x-ray photoelectron spectrometer scans showed that the coating was conformal around the individual fibers of the mat which demonstrated that the iCVD technique could be used to coat 3-dimensional objects. These previous iCVD studies only focused on the applications of the fluorinated coatings. This paper will conduct an in-depth mechanistic study of the process which encompasses the chemical structure of the deposited film, the adsorption isotherm of the monomer species, and the deposition kinetics of the iCVD fluoropolymer film. The aforementioned iCVD studies used commercial fluorinated methacrylate products having a distribution of pendant chain length from 5 to 13 perfluorinated carbons. This study however will use a fluorinated acrylate monomer with a single chain length, 1H,1H,2H,2H-perfluorodecyl acrylate (PFDA, $\text{CH}_2=\text{CHCOOCH}_2\text{CH}_2(\text{CF}_2)_7\text{CF}_3$), having the additional benefit that the free radical propagation rate constants are one order of magnitude larger for acrylates than for methacrylates.^{13,14} The PFDA monomer chain length which allow for the comparison of the experimental and theoretical chemical composition of the polymer films. The PFDA monomer has previously been vapor polymerized using continuous plasma polymerization and pulsed plasma polymerization.^{15,16} The continuous plasma created films that were damaged whereas the pulsed plasma could be optimized to produce films in which the fluorine moieties of the monomer remained intact. The highest deposition rate with the pulsed plasma however was found to be only 10 nm/min which is significantly lower than the deposition rates achieved in this work for the iCVD of PFDA (up to 375 nm/min).

Understanding the mechanistic aspects of the iCVD polymerization of PFDA will aid the optimization of the process and facilitate the application of the iCVD technique for coating more complex geometries. For instance, the surface modification of membranes has many potential applications.^{17,18} An increased knowledge of the iCVD polymerization mechanism of fluorinated acrylates could allow low surface energy iCVD coatings to be applied to a wide variety of substrates.

2.3 Experimental Methods

The PFDA films were deposited onto 100 mm diameter silicon wafers in a custom-built reactor. The reaction chamber is cylindrical with a diameter of 240 mm and a height of 33 mm. The top of the reaction chamber is covered with a removable transparent quartz plate (300 mm diameter, 25 mm thick). This transparent cover allows in situ monitoring of the deposition rate through the use of laser interferometry (JDS Uniphase He-Ne Laser).

The 1H,1H,2H,2H-Perfluorodecyl acrylate (PFDA) monomer (97%, Aldrich) and the tert-butyl peroxide initiator (98%, Aldrich) were used without further purification. The monomer was heated to 80°C and fed into the chamber through a heated mass flow controller (Model 1152C, MKS) and the initiator was kept at room temperature and fed into the chamber through another mass flow controller (Model 1479A, MKS). The reactor pressure was kept constant at 100 mTorr. Nichrome filaments (80% Ni/20% Cr) were resistively heated to 300°C. The distance between the filaments and the heat exchanger was kept at 29 mm. The silicon substrate was placed on a stage that was backside cooled using water from a recirculating chiller. A silicon wafer with

thermocouples bonded to the surface (Thermodynamic Sensors, Inc.) was used to measure the actual substrate temperature at the different chiller settings.

In order to study the effect of substrate temperature on the deposition rate, the substrate temperature was varied between 39°C-59°C while keeping all other variables constant. In order to study the effect of the monomer partial pressure on the deposition rate, the monomer flowrate was varied while keeping all other variables constant. Table 2-1 shows the details of these experiments. Experimental error bars were found by repeating the experiment three times and calculating the standard deviation.

Table 2-1: Process Conditions and Resultant Growth Rates for the iCVD PPFDA

Substrate Temperature Series									
Sample	Substrate Temp. (°C)	Monomer Flow Rate (sccm)	Initiator Flow Rate (sccm)	Total Pressure (Torr)	Monomer Partial Pressure, P _M (Torr)	Monomer Saturation Pressure, P _{sat} (Torr)	P _M /P _{sat}	Rate (nm/min)	Conversion (%)
TS1	39	0.31	0.82	0.10	0.03	0.11	0.24	144	49
TS2	44	0.31	0.82	0.10	0.03	0.16	0.17	72	24
TS3	54	0.31	0.82	0.10	0.03	0.32	0.09	20	7
TS4	59	0.31	0.82	0.10	0.03	0.44	0.06	8	3
Monomer Partial Pressure Series									
Sample	Substrate Temp. (°C)	Monomer Flow Rate (sccm)	Initiator Flow Rate (sccm)	Total Pressure (Torr)	Monomer Partial Pressure, P _M (Torr)	Monomer Saturation Pressure, P _{sat} (Torr)	P _M /P _{sat}	Rate (nm/min)	Conversion (%)
PM1	44	0.67	0.82	0.10	0.045	0.16	0.28	375	59
PM2	44	0.52	0.82	0.10	0.039	0.16	0.24	259	52
PM3	44	0.42	0.82	0.10	0.034	0.16	0.21	150	38
PM4	44	0.35	0.82	0.10	0.030	0.16	0.18	88	26
PM5	44	0.31	0.82	0.10	0.027	0.16	0.17	72	24
PM6	44	0.26	0.82	0.10	0.024	0.16	0.15	55	22
PM7	44	0.13	0.82	0.10	0.014	0.16	0.08	22	18

Fourier transform infrared spectroscopy (FTIR) (Thermo Nicolet Nexus 870) and X-ray photoelectron microscopy (XPS) (Kratos AXIS Ultra spectrometer with a monochromatized Al K α source) was used to study the chemical composition of the films. Variable angle spectroscopic ellipsometry (JA Woollam M-2000) was used to measure the thickness of the films. The refractive index of the films was between 1.36 and 1.37.

Contact angle measurements were conducted using a goniometer (Ramé-Hart Model 500). Atomic force microscopy (AFM) (Veeco Metrology Nanoscope IV/ Dimension 3100 Scanning Probe Microscope) was used to study the surface roughness of the polymer films. The molecular weight of the films was found by dissolving the films in 1,1,1,3,3,3-hexafluoro-2-propanol (HFIP) and then using gel permeation chromatography (GPC) (Waters Alliance Model 2690 with a Waters 410 Differential Refractive Index Detector and Viscotek Corporation Model T-60A dual detector module). There were three columns: two Shodex GPC HFIP-806M styrene-divinyl benzene columns and one Shodex GPC HFIP-804M styrene-divinyl benzene column.

A quartz crystal microbalance (QCM) (Sycon Instruments) with a 16 mm diameter gold-coated crystal sensor was used to conduct adsorption measurements. The QCM was placed inside the reactor chamber and the temperature was controlled using a chiller. The initiator flow was replaced with nitrogen and the filaments were kept off. In each run, monomer and nitrogen were flowed into the reactor and the pressure was increased to the reaction pressure (100 mTorr) and the adsorbed monomer volume was recorded. The monomer and nitrogen flow were then turned off and the pressure was decreased to the base pressure. The molecules now desorbed and the final adsorbed monomer volume was recorded. The amount of monomer adsorbed was taken to be the difference between the final and initial adsorbed monomer volume.

2.4 Results and Discussion

2.4.1 Material Characterization

The PPFDA film samples in Table 2-1 were characterized using FTIR. Figure 2-1 compares the FTIR spectra of the polymer film samples in the TS series (top) and the

PFDA liquid monomer (bottom). It can be seen that there is no significant difference found between the spectra of the polymer samples which indicates that varying the iCVD polymerization conditions does not change the local chemical bonding environment in the films. Figure 1a shows an enlarged view of the FTIR spectra in the region between 1900 cm^{-1} and 900 cm^{-1} . The sharp peak at 1741 cm^{-1} is caused by C=O stretching. This peak was used to normalize the intensity of the TS4 spectrum. The intensities of the other spectra reflect the different thicknesses of the films. Both the monomer and polymer spectra contain three strong, sharp absorbance peaks in the $1350\text{-}1120\text{ cm}^{-1}$ region. The sharp peaks at 1246 cm^{-1} and 1207 cm^{-1} are caused by the asymmetric stretching and symmetric stretching of the $-\text{CF}_2-$ moiety respectively.¹⁹ The sharp peak at 1153 cm^{-1} is caused by the $-\text{CF}_2\text{-CF}_3$ end group.²⁰ It can therefore be concluded that the iCVD PPFDA film retains the CF_2 and CF_3 moieties originating from the pendant functional group of the monomer. It is important to note that the peaks associated with the CF_2 and CF_3 groups remain as narrow in the iCVD polymer spectrum as they are in the monomer spectrum. In high energy plasma polymerizations, side reactions such as fragmentation and crosslinking lead to the broadening of the FTIR peaks to the extent that the individual peaks can no longer be resolved.¹⁵ The narrowness of the peaks in the iCVD polymer film therefore verifies the chemical homogeneity of the iCVD polymer film. The monomer spectrum in Figure 1a contains additional peaks at 1639, 1625, 1415, 1402, 1296, 1087, 1070, 990, and 968 cm^{-1} . These peaks are the characteristic absorbance bands for the C=C double bond.²¹ The polymer spectrum does not contain these peaks which is further evidence that the polymerization pathway during iCVD is through the double bond of the vinyl monomer.

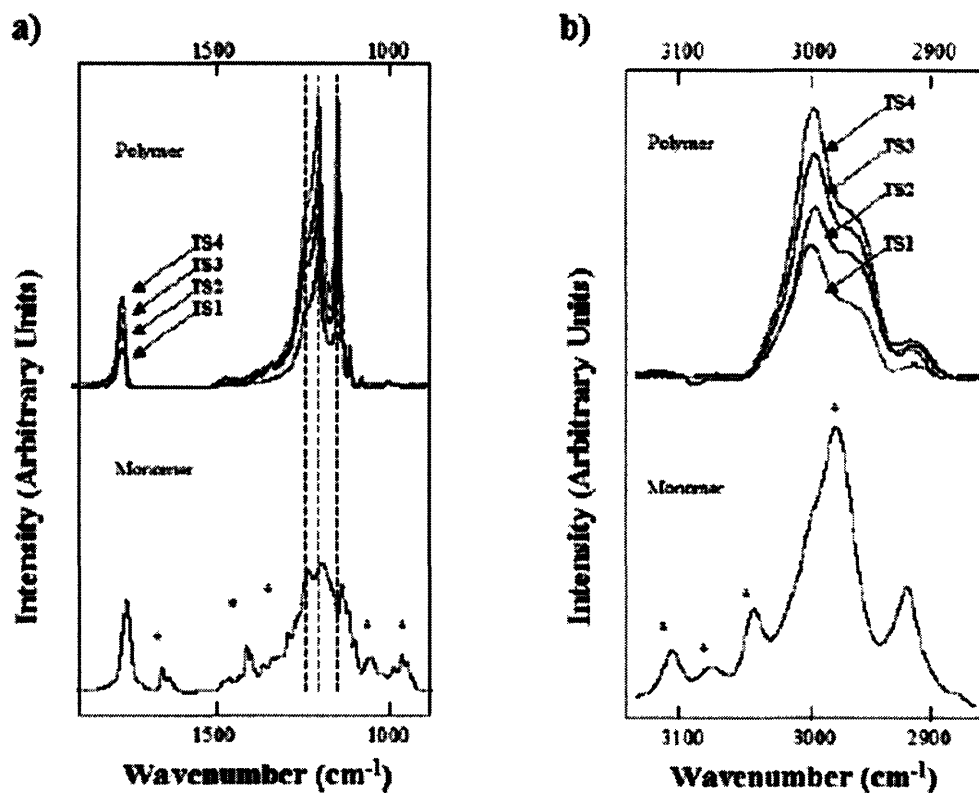


Figure 2-1: FTIR spectra of the iCVD PPFDA film samples in the TS series (top) and liquid PFDA monomer (bottom) in a) the region between 1900 cm^{-1} and 900 cm^{-1} and b) the region between 3150 cm^{-1} and 2800 cm^{-1} . The dashed lines represent the location of the CF_2 and CF_3 groups and the asterisks in both monomer spectra represent the location of the $\text{C}=\text{C}$ bond. The $\text{C}=\text{O}$ peak at 1741 cm^{-1} was used to normalize the intensity of the TS4 spectrum. The intensities of the other spectra reflect the different thicknesses of the films.

Figure 2-1b shows an enlarged view of the FTIR spectra of the polymer (top) and the monomer (bottom) in the region between 3150 cm^{-1} and 2800 cm^{-1} . The $\text{C}=\text{O}$ peak at 1741 cm^{-1} was again used to normalize the intensity of the TS4 spectrum. The absorbance peaks in the monomer spectrum between 3090-3075 cm^{-1} and 3020-2980 cm^{-1} are associated with the $\text{C}=\text{C}$ double bond.²¹ The polymer spectrum does not contain these peaks but it does contain strong peaks in the region 2969-2965 cm^{-1} , 2936-2912 cm^{-1} , and

2863-2843 cm^{-1} which are associated with the C-H stretching and CH_2 vibrations on a saturated carbon atom.¹⁹ This verifies that the iCVD polymerization process converts the unsaturated carbon from the vinyl bond of the monomer into polymerized chains with saturated carbons as has been observed during the iCVD polymerization of other monomers.²²

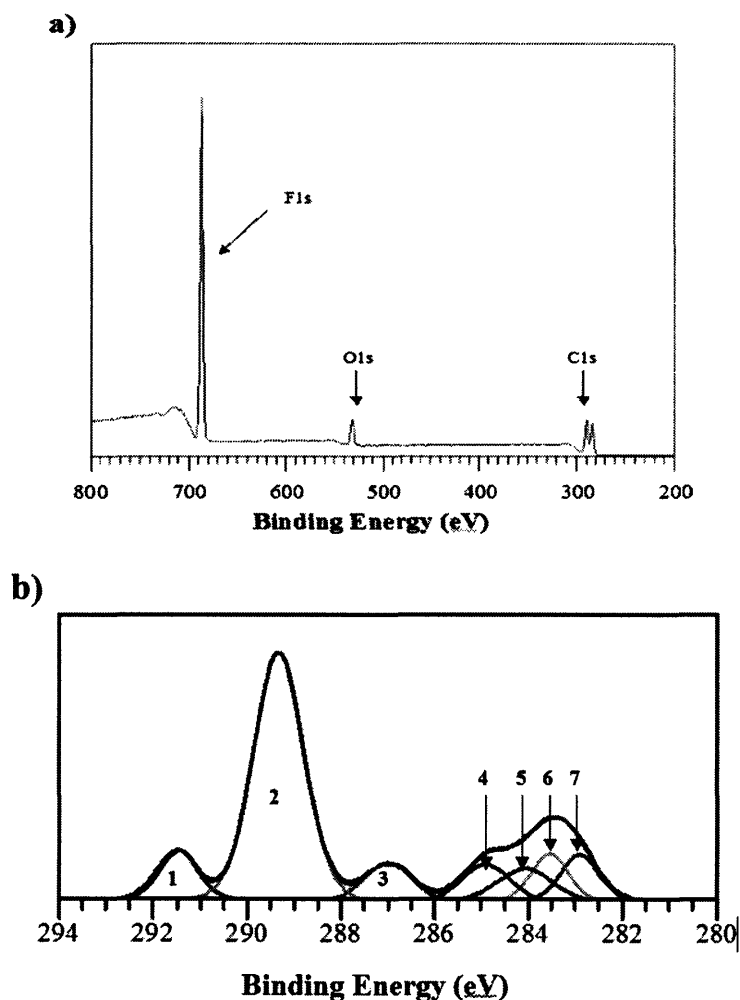


Figure 2-2: XPS spectra of the iCVD PPFDA film sample TS1. a) Survey scan showing the atomic concentration of fluorine, oxygen, and carbon in the polymer film. b) High resolution scan of the C 1s peak with seven resolved peaks.

Figure 2-2a shows the XPS survey scan of the PPFDA film sample TS1 and Table 2-2 shows the atomic concentration percentages calculated from the survey scan. Excellent agreement is observed between these experimentally obtained percentages and the theoretical values calculated from the chemical formula of the monomer. Figure 2-2b shows the corresponding high resolution C 1s XPS spectrum. The spectrum can be described using seven bonding environments expected solely due to vinyl polymerization of the monomer (Table 2-3). Again, the agreement between the experimental and theoretical area percentages for the $-CF_2-$ and CF_3 groups show that the structure of the monomer unit, including that of the functional pendant group, is completely maintained during iCVD polymerization.

The static and dynamic water contact angles were measured on each coated sample in Table 2-1. There was no significant difference between the samples. The static contact angle was found to be $120.8^\circ \pm 1.2^\circ$. This is the maximum contact angle that can be achieved on a flat hydrophobic surface²³ since static contact angles higher than 120° can only be achieved through the addition of surface roughness. The consistency of the contact angle measurements from sample to sample suggests that all the films have low surface roughness. Indeed, AFM measurements on each coated sample in Table 2-1 confirmed the low surface roughness (14.9 nm – 19.8 nm RMS). The advancing and receding contact angles were found to be $132.3^\circ \pm 1.3^\circ$ and $99.5^\circ \pm 1.3^\circ$ respectively. These values agree with those found for polymeric films that contain CF_3 end groups.¹¹

Polymers made from fluorinated monomers are not very soluble in common solvents such as tetrahydrofuran.²⁴ The PPFDA films were therefore dissolved in a fluorinated solvent, 1,1,1,3,3,3-hexafluoro-2-propanol (HFIP), in order to get GPC

results. Table 2-4 shows the weight average molecular weight, M_w , and polydispersity of samples that vary with substrate temperature and monomer partial pressure. It can be seen that the molecular weight increases with decreasing substrate temperature and increases with increasing monomer partial pressure. The polydispersity ranges between 1.9 - 2.6 with no observable trend with respect to substrate temperature or monomer partial pressure. This range in polydispersity has also been observed for the iCVD polymerization of other acrylates.²⁵ The ability to dissolve the PPFDA film in HFIP solvent supports the hypothesis that there is limited crosslinking during the iCVD process.

Table 2-2: Atomic Percentages from XPS Survey Scan

Theoretical			
Atomic %	Carbon	Oxygen	Fluorine
	40.63	6.25	53.13
Experimental			
Atomic %	Carbon	Oxygen	Fluorine
	40.6 +/- 0.7	5.7 +/- 0.7	53.7 +/- 0.8

Table 2-3: Atomic Percentages of Carbon Environments from C 1s XPS Spectra

		Theoretical²⁶		Experimental	
		Binding Energy (eV)	Area (%)	Binding Energy (eV)	Area (%)
1	-C [*] F ₃	293.3	7.7	293.5	7.7 +/- 0.1
2	-C [*] F ₂ -	291.2	53.8	291.3	53.7 +/- 0.2
3	-C [*] =O	289.2	7.7	289.0	7.6 +/- 0.3
4	-CH ₂ -C [*] H ₂ -CF ₂ -	286.8	7.7	286.9	7.5 +/- 0.7
5	-O-C [*] H ₂ -CH ₂ -	286.7	7.7	286.1	7.7 +/- 0.7
6	-C [*] H-CO-	285.7	7.7	285.5	7.8 +/- 0.7
7	-C-C [*] H ₂ -C-	285.0	7.7	284.9	7.8 +/- 0.7

Table 2-4: Weight Average Molecular Weight From GPC Measurements

Substrate Temperature Series			
Substrate Temperature (°C)	P_M/P_{sat}	M_w	Polydispersity
44	0.38	177300	2.27
49	0.27	114300	2.63
54	0.20	42800	2.01
Monomer Partial Pressure Series			
Substrate Temperature (°C)	P_M/P_{sat}	M_w	Polydispersity
39	0.50	127800	1.89
39	0.45	109300	1.91
39	0.38	91100	1.91

2.4.2 Effect of Substrate Temperature

Figure 3 shows the deposition rate as a function of substrate temperature plotted in an Arrhenius form (Series TS, Table 2-1). It can be seen that the deposition rate increases with decreasing substrate temperature. The maximum rate for this series (144 nm/min) was achieved at the lowest substrate temperature used (39°C). The monomer conversion for the polymerization was calculated at each substrate temperature by dividing the mass of the deposited film by the mass of the monomer feed. Table 2-1 shows that the conversion for series TS ranged between 3% at the highest substrate temperature and 49% at the lowest substrate temperature. Previous QCM experiments have shown that decreasing the substrate temperature increases the monomer surface concentration and thereby increases the deposition rate and conversion.²⁷

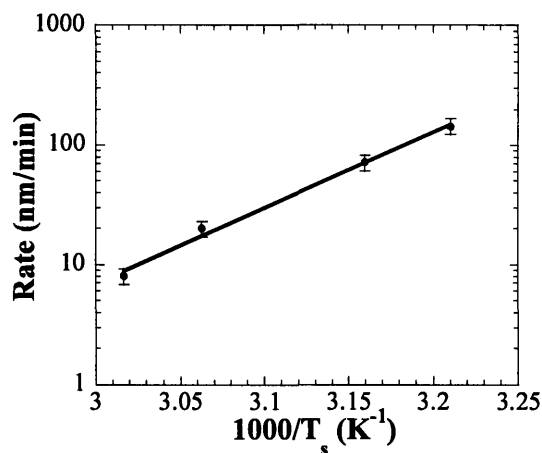


Figure 2-3: Deposition rate as a function of the substrate temperature plotted in an Arrhenius form where the solid line represents the results of a linear regression to the data. (Series TS, Table 2-1)

Although the monomer partial pressure is the same for all the points in this series, the saturation pressure changes with substrate temperature according to the Clausius-Clapeyron equation:²⁸

$$P_{sat} = A \exp[-\Delta H_{vap} / RT_{sub}] \quad (1)$$

The saturation pressure of PFDA at 25°C and 334°C is 0.0559 Torr and 760 Torr respectively.²⁹ The heat of vaporization estimated using equation 1 is 57.3 kJ/mol. This information can be used to find the saturation pressure at each substrate temperature. It is important to note that the derivation of the Clausius-Clapeyron assumes that the heat of vaporization is independent of pressure and temperature. This might cause error in the calculation of the saturation pressures. Table 2-1 shows the calculated saturation pressure at each substrate temperature and it can be seen that the deposition rate increases with increasing P_m/P_{sat} . At these low values of P_m/P_{sat} (<0.24), it has previously been shown that the iCVD deposition rate is second order with respect to the monomer concentration and therefore the apparent activation energy found from the Arrhenius plot of the

deposition rate versus substrate temperature should be equal to twice the negative heat of desorption ($E_a = -2\Delta H_{des}$).²⁵ The apparent activation energy found from the slope of the linear regression line in Figure 2-3 is -121.4 ± 3.4 kJ/mol and therefore ΔH_{des} is found to be 60.7 ± 1.7 kJ/mol. This heat of desorption is of the same order of magnitude as that of ethyl acrylate (39.7 ± 2.4).²⁵ The higher value found for PFDA might be a result of the higher intermolecular dispersion forces of this larger monomer.

2.4.3 Effect of Monomer Partial Pressure

Figure 2-4 shows the plot of the deposition rate as a function of P_m/P_{sat} at a constant substrate temperature of 44°C (Series PM, Table 2-1). Since the substrate temperature is constant, the saturation pressure is constant and the only variable being changed is P_m . It can be seen that the deposition rate increases with P_m/P_{sat} which is consistent with the data for series TS (Table 2-1). A deposition rate as high as 375 nm/min is achieved at the highest P_m/P_{sat} . Table 2-1 shows that the conversion for series PM ranged between 18% at the lowest P_m/P_{sat} and 49% at the highest P_m/P_{sat} .

This deposition rate of PPFDA is higher than the deposition rate found with smaller acrylates because the PFDA monomer is less volatile and therefore adsorbs onto the surface in greater quantities than higher vapor pressure monomers at equal monomer partial pressures.²⁵ Also, the deposition rate achieved for the iCVD polymerization of PFDA is much higher than the deposition rate found in the pulsed plasma polymerization of the same monomer (10nm/min).¹⁵ The slow deposition rates found in plasma polymerization are due to the complexity of the plasma process. The high energy of the plasma partially breaks apart the monomer, reducing the concentration available for polymerization. In contrast, the iCVD process only breaks the initiator and leaves the

monomer completely intact. Additionally, there is a competition between etching and deposition in plasma processes³⁰ where the iCVD process involves only deposition and no etching.

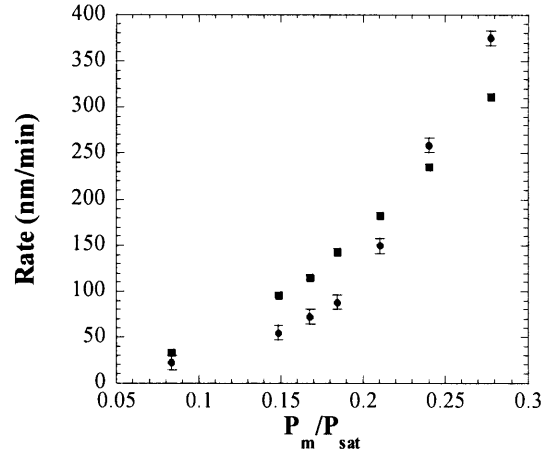


Figure 2-4: Deposition rate (circles) as a function of monomer partial pressure at a constant substrate temperature of 44°C. (Series PM, Table 2-1) The squares represent the predicted values of the kinetic model.

In order to further study this set of data, QCM measurements were conducted at this constant substrate temperature. It can be assumed that these are equilibrium measurements since sufficient time was allowed for the QCM to stabilize to a constant value. Figure 2-5 shows the volume of monomer adsorbed on a square centimeter of surface area, V_{ad} , as a function P_m/P_{sat} . It can be seen that the monomer surface concentration increases with increasing P_m/P_{sat} . This QCM data can be fitted to the BET equation:³¹

$$V_{ad} = \frac{V_{ml}c(P_m / P_{sat})}{(1 - P_m / P_{sat})[1 - (1 - c)(P_m / P_{sat})]} \quad (2)$$

$$c \approx \exp[(\Delta H_{des} - \Delta H_{vap}) / RT_{sub}] \quad (3)$$

where V_{ml} is the volume of a monolayer adsorbed on a square centimeter of surface area. Fitting the QCM data to equation 2 yields the dashed line in Figure 2-5 where c is 3.3 and V_{ml} is 236.4 pL/cm^2 . This monolayer volume is greater than that found for ethyl acrylate (145.6 pL/cm^2)²⁵ which is to be expected since the PDFFA monomer is larger than ethyl acrylate. Since the substrate temperature is constant, the value for c can also be calculated using equation 3. In the previous section, the heat of desorption was found to be 60.7 kJ/mol using Figure 2-3 and the heat of vaporization was found to be 57.3 kJ/mol using equation 1. The calculated value for c using equation 3 is therefore 3.6. This experimental c value is to within 10% of the c value found from the regression to the BET isotherm (Figure 5). This verifies that the deposition rate data is reasonably consistent with the data from the QCM measurements.

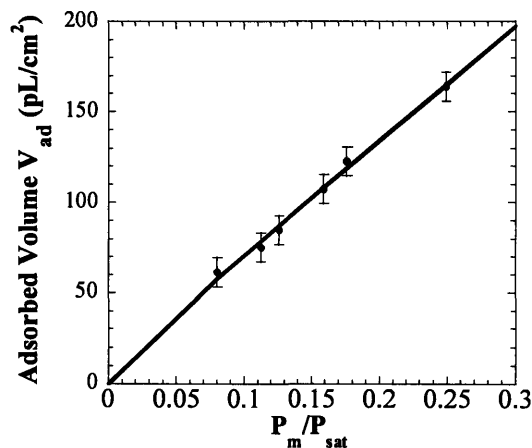


Figure 2-5: QCM measurements of the monomer adsorption as a function of monomer partial pressure at a constant crystal temperature of 44°C . The solid line represents the regression to the BET isotherm.

2.4.4 Kinetics

Figure 2-6 shows the reaction steps proposed to take place on the substrate surface during the iCVD polymerization process and their associated reaction rate constants.³² The steps are similar to traditional free radical polymerization in the liquid phase. Initiation occurs when the initiator free radical attacks the vinyl bond of the monomer. The resulting radical then adds to another vinyl monomer during the propagation step. Termination can occur when two of the propagating radicals react. Since there is a high concentration of initiator molecules used in these experiments (I/M ratio ~2), termination can also occur by primary radical termination and primary radical recombination.

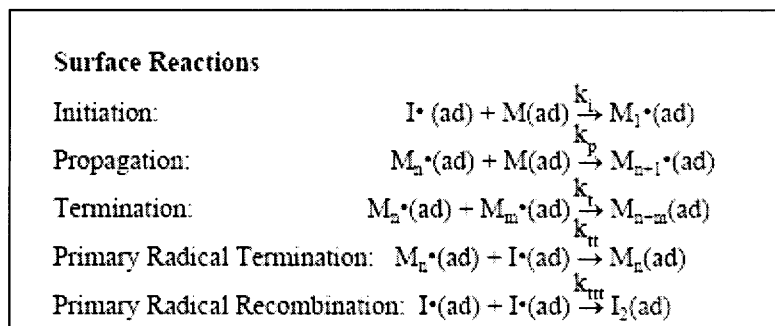


Figure 2-6: Details of the reaction steps that take place on the substrate surface during iCVD polymerization where I is the initiator and M is the monomer.

The kinetic rate constants for the iCVD polymerization of PDFFA can be found using a mathematical model that was derived elsewhere for the iCVD polymerization of butyl acrylate.³² The model uses a multiresponse parameter estimation based on minimizing the determinant criterion. Figure 4 shows the results of the kinetic model of

the iCVD polymerization of PFDA. Table 2-5 compares the kinetic parameters found for the iCVD polymerization of butyl acrylate to that of the PFDA. It is seen that the rate constants for PFDA are of the same order of magnitude as those for butyl acrylate. The reaction rate constants are also similar to those found in literature for the free radical polymerization of acrylates in the liquid phase.³³ As with the butyl acrylate experiments, k_{tt} and k_{ttt} are higher in magnitude than k_t . This is because primary radicals are smaller than polymer radicals and can therefore terminate a polymer radical faster. Since PFDA is larger than butyl acrylate, it is reasonable that the k_t is smaller for PFDA than butyl acrylate.

Table 2-5: Comparison of iCVD rate constants for butyl acrylate and PFDA

Parameter (L/mol·s)	butyl acrylate ³²	PFDA
k_i	4990	7494 +/- 30
k_p	15540	11418 +/- 200
k_t	9.8×10^5	2.3×10^4 +/- 1×10^3
k_{tt}	6.89×10^7	10.66×10^7 +/- 4×10^6
k_{ttt}	7.41×10^8	1.5×10^9 +/- 1×10^8

2.5 Conclusions

Initiated chemical vapor deposition (iCVD) was successfully utilized to create thin films of poly(1H,1H,2H,2H-perfluorodecyl acrylate) (PPFDA). The XPS survey and C 1s scans both showed that the iCVD PPFDA film has the same stoichiometric composition as the monomer and therefore all the fluorine moieties have been kept intact. FTIR analysis of the polymer film showed the complete disappearance of the vinyl bonds and the narrow FTIR peaks and the GPC measurements indicated that there was no measurable crosslinking. The water contact angles measured on the PPFDA films were as high as those that can be achieved on a flat surface.

The mechanistic aspects of the iCVD polymerization of PFDA were studied. It was found that deposition kinetics followed the same trends with respect to substrate temperature and monomer partial pressure as that of the iCVD polymerization of other nonfluorinated vinyl monomers. The adsorption isotherm of the PFDA monomer was similar to the adsorption isotherms of other vinyl monomers and was found to follow the BET isotherm. The c value measured from the adsorption isotherm agreed well with the c value calculated from the deposition rate data which verifies that the kinetic data and the thermodynamic data in this study are consistent with each other. The rate constants for the iCVD polymerization of PFDA were derived using a previously published kinetic model and were found to be of the same order of magnitude as those derived for the iCVD polymerization butyl acrylate. This verifies that the iCVD polymerization of PFDA follows the kinetic models previously developed for the iCVD platform. The mechanistic data found in this paper can now be used to study the surface polymerization of PFDA onto more complex geometries.

2.6 Acknowledgments

We would like to thank the DuPont MIT Alliance for financial support. We would especially like to thank Dr. Yefim Brun and Dr. Vivek Kapur for help with the GPC measurements. We thank Dr. Kenneth K. S. Lau for helpful discussions. We would also like to thank the MIT CMSE shared facilities supported in part by the MRSEC program of the National Science Foundation under award number DMR 02-13282.

2.7 References

- (1) Mao, Y.; Gleason, K. K. *Langmuir* **2006**, *22*, 1795-1799.
- (2) Lau, K. K. S.; Bico, J.; Teo, K. B. K.; Chhowalla, M.; Amaratunga, G. A. J.; Milne, W. I.; McKinley, G. H.; Gleason, K. K. *Nano Lett.* **2003**, *3*, 1701-1705.
- (3) Mao, Y.; Gleason, K. K. *Langmuir* **2004**, *20*, 2484-2488.
- (4) Chan, K.; Gleason, K. K. *Langmuir* **2005**, *21*, 8930-8939.
- (5) Feng, L.; Li, S.; Li, Y.; Li, H.; Zhang, L.; Zhai, J.; Song, Y.; Liu, B.; Jiang, L.; Zhu, D. *Adv. Mater.* **2002**, *14*, 1857-1860.
- (6) Chen, W.; Fadeev, A. Y.; Hsieh, M. C.; Oner, D.; Youngblood, J.; McCarthy, T. J. *Langmuir* **1999**, *15*, 3395-3399.
- (7) Furukawa, Y.; Kotera, M. *J. Appl. Polym. Sci.* **2003**, *87*, 1085-1091.
- (8) McCord, M. G.; Hwang, Y. J.; Qiu, Y.; Hughes, L. K.; Bourham, M. A. *J. Appl. Polym. Sci.* **2003**, *88*, 2038-2047.
- (9) Thunemann, A. F.; Lieske, A.; Paulke, B.-R. *Adv. Mater.* **1999**, *11*, 321-324.
- (10) Park, I. J.; Lee, S. B.; Choi, C. K.; Kim, K. J. *J. Colloid Interface Sci.* **1996**, *181*, 284-288.
- (11) Mao, Y.; Gleason, K. K. *Macromolecules* **2006**, *39*, 3895-3900.
- (12) Ma, M.; Mao, Y.; Gupta, M.; Gleason, K. K.; Rutledge, G. C. *Macromolecules* **2005**, *38*, 9742-9748.
- (13) Beuermann, S.; Paquet Jr., D. A.; McMinn, J. H.; Hutchinson, R. A. *Macromolecules* **1996**, *29*, 4206-4215.
- (14) Hutchinson, R. A.; Beuermann, S.; Paquet Jr., D. A.; McMinn, J. H.; Jackson, C. *Macromolecules* **1998**, *31*, 1542-1547.
- (15) Coulson, S. R.; Woodward, I.; Badyal, J. P. S.; Brewer, S. A.; Willis, C. *Chem. Mater.* **2000**, *12*, 2031-2038.
- (16) Coulson, S. R.; Woodward, I.; Badyal, J. P. S.; Brewer, S. A.; Willis, C. *Langmuir* **2000**, *16*, 6287-6293.
- (17) Letant, S. E.; Hart, B. R.; Van Buuren, A. W.; Terminello, L. J. *Nat. Mater.* **2003**, *2*, 391-395.

-
- (18) Chen, P.; Mitsui, T.; Farmer, D. B.; Golovchenko, J.; Gordon, R. G.; Branton, D. *Nano Lett.* **2004**, *4*, 1333-1337.
- (19) Lin-Vien, D.; Colthup, N. B.; Fateley, W. G.; Grasselli, J. G. *The Handbook of Infrared and Raman Characteristic Frequencies of Organic Molecules*; Academic Press: San Diego, 1991.
- (20) Szymanski, H.A.; Erickson, R. E. *Infrared Band Handbook*, 2nd edition; IFI/Plenum: New York, 1970.
- (21) Gunzler, H.; Gremlich, H.-U. *IR Spectroscopy*; Wiley-VCH: Weinheim, 2002.
- (22) O'Shaughnessy, W. S.; Gao, M.; Gleason, K. K. *Langmuir* **2006**, *22*, 7021-7026.
- (23) Lafuma, A.; Quere, D. *Nat. Mater.* **2003**, *2*, 457-460.
- (24) Anton, D. *Adv. Mater.* **1998**, *10*, 1197-1205.
- (25) Lau, K. K. S.; Gleason, K. K. *Macromolecules* **2006**, *39*, 3688-3694.
- (26) Beamson, G.; Briggs, D. *High Resolution XPS of Organic Polymers*; John Wiley & Sons: Chichester, 1992.
- (27) Chan, K.; Gleason, K. K. *Macromolecules* **2006**, *39*, 3890-3894.
- (28) Engel, T.; Reid, P. *Thermodynamics, Statistical Thermodynamics, & Kinetics*; Benjamin Cummings: San Francisco, 2006.
- (29) From SciFinder Scholar © American Chemical Society. Calculated Using Advanced Chemistry Development (ACD/Labs) Software V8.14 for Solaris (© 1994-2006 ACD/Labs).
- (30) d'Agostino, R. *Plasma Deposition, Treatment, and Etching of Polymers*; Academic Press: Boston, 1990.
- (31) Adamson, A. W. *Physical Chemistry of Surfaces*, 5th edition; John Wiley & Sons: New York, 1990.
- (32) Lau, K. K. S.; Gleason, K. K. *Macromolecules* **2006**, *39*, 3695-3703.
- (33) Odian, G. *Principles of Polymerization*, 4th edition; Wiley-Interscience: Hoboken, 2004.

Chapter Three:
Large Scale Initiated Chemical Vapor Deposition
of Poly(glycidyl methacrylate) Thin Films

Published in Thin Solids Films:

Malancha Gupta and Karen K. Gleason. "Large Scale Initiated Chemical Vapor Deposition of Poly(glycidyl methacrylate) Thin Films", *Thin Solid Films*, 515, 1579-1584, 2006.

3.1 Abstract

The initiated Chemical Vapor Deposition (iCVD) of poly(glycidyl methacrylate) (PGMA) was scaled up using dimensionless analysis. In the first stage, PGMA was deposited onto a large stationary substrate and a deposition rate as high as 85 nm/min was achieved. It was found that the deposition rate increases with increasing filament temperature whereas the deposition rate and the number-average molecular weight decrease with increasing substrate temperature. In the second stage, PGMA was deposited onto a moving substrate. At speeds between 20 mm/min and 60 mm/min, the deposition rate on the moving substrate was found to be equal to the deposition rate on the stationary substrate. Fourier transform infrared spectroscopy showed that the epoxide functionality of the PGMA films was retained during the iCVD process. Since the iCVD polymerization of different vinyl monomers all use similar parameters, this scale up can be applied to the scale up of other vinyl monomers such as 2-hydroxyethyl methacrylate and perfluoroalkyl ethyl methacrylate.

Initiated chemical vapor deposition (iCVD) is a low energy vapor deposition process (0.01 W/cm^2) that can be used to produce linear polymers in which the pendant chemical moieties are kept intact [7]. iCVD has been used to polymerize a wide variety of vinyl monomers such as glycidyl methacrylate [8], 2-hydroxyethyl methacrylate [9], and perfluoroalkyl ethyl methacrylate [10,11]. Tert-butyl peroxide is used as the initiator. The proposed polymerization mechanism is the classical free radical polymerization mechanism of vinyl monomers (see Figure 3-1). Monomer and initiator gases are fed into a vacuum chamber where resistively heated wires are used to thermally decompose the initiator molecules into free radicals. The free radicals then attack the vinyl bonds of the monomer molecules. Propagation occurs on the surface of a cooled substrate. The cool substrate temperature promotes adsorption of the monomer and allows thermally sensitive substrates to be coated.

The aforementioned iCVD polymerizations have all been conducted in small-scale reactors (diameters less than 200 mm) in which the substrate remains stationary and the deposition occurs between transient pump down and pump up periods. These small-scale processes can be scaled up by either using a larger stationary substrate or by using a roll-to-roll process in which uncoated substrate continuously enters the reaction zone at a steady rate and exits as coated. The roll-to-roll process allows for the production of realistic size samples that can be easily tested for various applications. The roll-to-roll process also saves the time it takes to load the substrate, pump down to the reaction pressure, heat the filament, and pump back up. For example, the small-scale iCVD polymerizations take approximately 30 minutes to load the sample and pump down and

30 minutes to unload the sample and shutdown. The actual deposition takes only a few minutes.

There has been significant work in scaling up inorganic vapor deposition processes. Large area deposition of amorphous silicon has been studied in a plasma roll-to-roll reactor [12,13], a plasma in-line deposition system [14], and a large area hot wire CVD apparatus [15]. An in-line deposition system has also been used to create films containing copper, indium, gallium, and selenium [16]. The pulsed laser deposition of tantalum pentoxide films has been scaled up to larger areas through the use of a rotating substrate [17].

The goal of this work is to scale up the iCVD polymerization of glycidyl methacrylate. Poly(glycidyl methacrylate) (PGMA) has many uses since it contains an epoxy group that can be attached to various chemical groups such as amines and acids through a ring-opening reaction [18,19]. Since the iCVD polymerization of different vinyl monomers all use similar parameters, this scale up can be applied to the scale up of other vinyl monomers.

3.3 Experimental Details

The reactions were carried out in a 0.16 m³ roll-to-roll vacuum chamber that contains one unwinder roll, three spreader rolls to prevent wrinkling of the web, one tension roll, and one rewinder roll (PLASMAtech model V-160GK-RT). The maximum length of the roll is 30 cm and the maximum diameter of the roll is 16 cm. The chamber was custom modified in order to reproduce the gas flow profiles and filament to substrate standoff of smaller-scale iCVD reactors. A vertical 35 cm by 43 cm stainless steel baffled heat exchanger was placed between the filament array and the rolls. The setup is shown in

Figure 3-2. The heat exchanger served to cool the substrate and to physically force the inlet gases to flow along the direction of the substrate and exit uniformly. The width of the heat exchanger spans the entire depth of the reaction chamber. The monomer and initiator gases were uniformly distributed across the entire width of the substrate using a distributor tube that was 30 cm long and 1.3 cm in diameter and contained ten 1 millimeter holes. A square filament array holder was custom designed to be wider (35 cm) than the roll width (30 cm) in order to ensure that the edges of the roll will get exposure to the filaments and will therefore have the same thickness as the rest of the substrate. The filaments were strung across the width of the substrate in order to achieve uniformity across the width of the substrate, perpendicular to the direction of gas flow. As the substrate moves along, its entire width will be exposed to each separate filament.

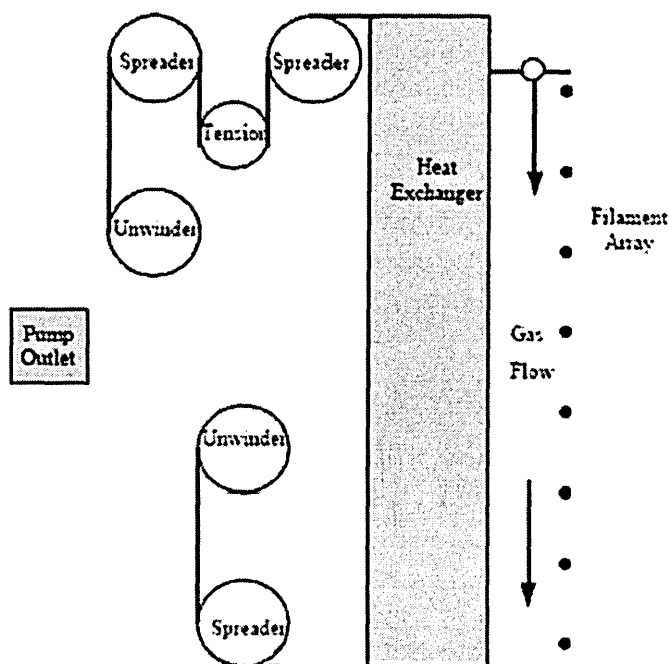


Figure 3-2: Schematic of the custom modified iCVD roll-to-roll system.

The glycidyl methacrylate (GMA) monomer (99%, Polysciences, Inc.) and the tert-butyl peroxide initiator (98%, Aldrich) were used without further purification. The monomer was heated to 75°C and fed into the chamber through a heated line at a flow rate of 4.5 sccm. The initiator was kept at room temperature and fed into the chamber through another line at a flow rate of 4.5 sccm. The reactor pressure was kept constant at 40 Pa. Nichrome filaments (80% Ni/20% Cr) were resistively heated to temperatures between 180-250°C. The distance between the filaments and the heat exchanger was kept at 2.5 cm. The heat exchanger settings were varied between 15-35°C. The substrate temperature will depend on both the heat exchanger temperature and the filament temperature. A silicon wafer with thermocouples bonded to the surface (Thermodynamic Sensors, Inc.) was used to measure the substrate temperature at different heat exchanger settings and filament temperatures (see Figure 3-3).

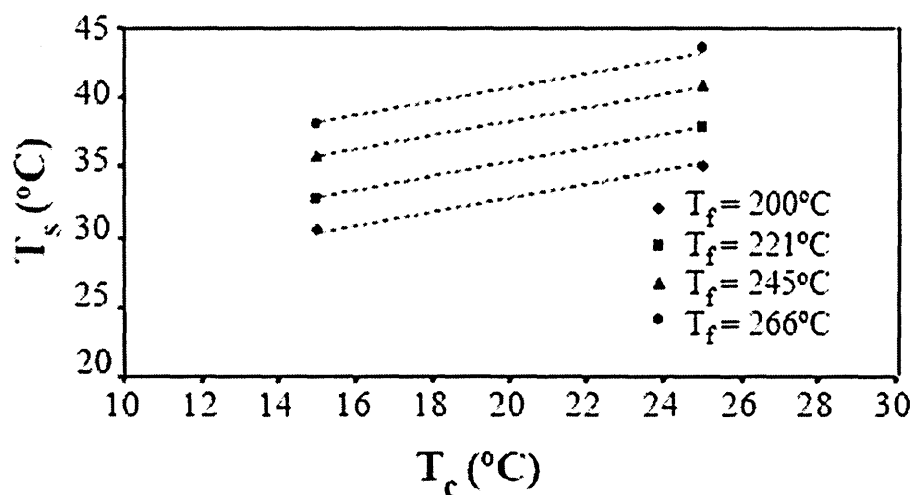


Figure 3-3: Substrate temperature (T_s) as a function of the heat exchanger setting (T_c) and filament temperature (T_f).

Fourier transform infrared spectroscopy (Thermo Nicolet Nexus 870) was used to study the chemical composition of the films. Variable angle spectroscopic ellipsometry (JA Woollam M-2000) was used to measure the thickness of the films. The number-average molecular weight of the films was found by dissolving the films in tetrahydrofuran and then using gel permeation chromatography (GPC)(Waters 1515 Isocratic High Performance Liquid Chromatography pump and Waters 2414 Refractive Index Detector). Polymethylmethacrylate standards (Polymer Laboratories) were used for the GPC calibration.

3.4 Results and Discussion

3.4.1 Dimensionless Analysis

In order to accurately scale up the iCVD process, a dimensionless analysis of the transport properties must be performed in order to ensure that convection and diffusion have the same contribution in both the small-scale reactor and the roll-to-roll reactor [20]. The Reynolds number, thermal Peclet number, and mass Peclet number are the dimensionless numbers that measure the importance of convection relative to diffusion:

$$\text{Re} = \frac{UL}{\nu} \quad (1)$$

$$\text{Pe}_{thermal} = \frac{UL}{\alpha} \quad (2)$$

$$\text{Pe}_{mass} = \frac{UL}{D} \quad (3)$$

Where U is the gas velocity, L is the characteristic length scale, and ν , α , and D are the momentum, thermal, and mass diffusivities respectively. The gas velocity is calculated by solving for the flow profile within the reactor. As explained in the experimental section, the roll-to-roll reaction chamber was custom modified in order to reproduce the same gas

flow profile as that in the small-scale reactor. The gas-phase initiator and monomer molecules are distributed between the heat exchanger and the filament array. A boundary layer is created around each filament. The spacing between the filaments was chosen to be approximately twice the boundary layer thickness so that the filament array acts as a flat plate [21]. The energy, mass, and momentum diffusivities are calculated using the kinetic theory for gases [22].

In order to keep the dimensionless numbers (1)-(3) approximately the same in the roll-to-roll reactor as that in the small-scale reactor used for the iCVD of poly(glycidyl methacrylate)[23], the filament to substrate standoff was kept the same to retain the same characteristic length scale and the appropriate gas feed rate was chosen. Changing the reactor pressure does not affect the dimensionless numbers since the gas diffusivities and the flow velocity are both inversely proportional to the reactor pressure. The reactor pressure does however influence the residence time. The appropriate reactor pressure was chosen to keep the residence time the same in both the reactors. Table 3-1 lists the reactor conditions and the values of important transport properties for both the small-scale reactor and the roll-to-roll reactor.

It is important to note that the roll-to-roll reactor is a vertical reactor whereas the small-scale reactor is a horizontal reactor. The free convection flow pattern of a gas enclosed between two parallel horizontal walls is not equivalent to the free convection flow pattern of a gas enclosed between two vertical walls. In a horizontal setup, free convection currents do not occur as long as the temperature of the upper wall is greater than the temperature of the lower wall since the less dense gas layers are located above the denser gas layers. In a vertical setup, there is no stable state since free convection

forces the fluid to move upward along the heated wall and downward along the cooled wall [24].

	Small-Scale Reactor	Roll-to-Roll Reactor
Pressure	0.5 Torr	0.3 Torr
Maximum Velocity	0.015 m/s	0.020 m/s
Residence Time	14 s	15 s
Momentum Diffusivity	0.0021 m ² /s	0.0036 m ² /s
Thermal Diffusivity	0.0021 m ² /s	0.0036 m ² /s
Mass Diffusivity	0.0022 m ² /s	0.0037 m ² /s
Reynolds Number	0.17	0.15
Peclet Number (thermal)	0.17	0.15
Peclet Number (mass)	0.16	0.14

Table 3-1: List of reactor conditions and transport properties for the polymerization of glycidyl methacrylate in both the small-scale reactor and the roll-to-roll reactor.

The scale up of the iCVD polymerization of glycidyl methacrylate was divided into two main stages using the reactor conditions in Table 3-1. In the first stage, the PGMA was deposited onto a large stationary substrate. In the second stage, the PGMA was deposited onto a moving substrate.

3.4.2 Large Area Deposition

The temperature of the solution is the only temperature that characterizes the reaction rate in most liquid-phase polymerizations. In the iCVD polymerization process however there are two temperatures that characterize the reaction rate. The filament temperature controls the breakdown of the gas-phase initiator into free radicals and the substrate temperature controls the adsorption of growth species, such as the initiator

radicals and monomer molecules onto the surface. These temperature effects were studied in the roll-to-roll reactor in order to compare the trends to those found in the small-reactors.

The filament temperature was varied between 180-250°C while keeping the substrate at a constant temperature of 35°C. Figure 3-4 shows a plot of the deposition rate as a function of filament temperature plotted in an Arrhenius form. It can be seen that the deposition rate increases with increasing filament temperature. The amount of GMA consumed in the reactor was calculated by dividing the mass of the deposited film by the mass of the GMA monomer feed. Since only 2% of the GMA monomer feed is consumed even at the highest deposition rate, it can be assumed that the concentration of GMA in the reactor is constant. It can also be assumed that the growth kinetics is zero order with respect to the initiator as demonstrated by previous experiments in which the initiator to monomer ratio was greater than 0.32 [8]. Under these assumptions, the deposition rate is proportional to the overall reaction rate constant and therefore the Arrhenius plot can be used to find the overall activation energy. The apparent activation energy from the slope of the linear regression line is 28.2 +/- 2.3 kJ/mol. The exponential increase in deposition rate with temperature has been seen in the small-scale iCVD polymerizations [8,25]. The filament temperature controls the gas-phase reactions only. The breakdown of the initiator into free radicals is the main process believed to occur in the gas-phase [26]. At higher filament temperatures, more initiator radicals are formed and the deposition rate is therefore increased. The plot also shows that a deposition rate as high as 85 nm/min can be achieved when the filament temperature is 245°C. At the same filament temperature of 245°C and at a 1:1 initiator to monomer ratio, the PGMA deposition rate in the small-

scale reactor was found to be about 90 nm/min [8]. It can therefore be concluded that the iCVD process can be accurately scaled up onto a large area substrate by using the dimensionless analysis listed in Table 3-1.

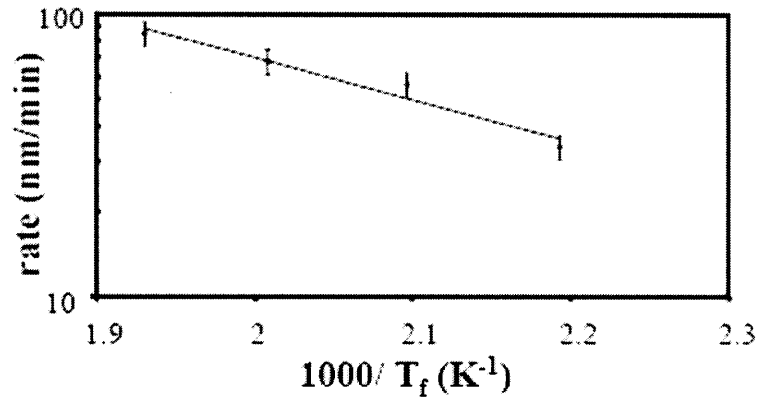


Figure 3-4: Deposition rate as a function of the filament temperature plotted in an Arrhenius form. The substrate temperature is held constant at 35 °C.

In order to study the effects of the substrate temperature, the substrate temperature was varied between 35°-46° while keeping the filament temperature at a constant temperature of 245 °C. Figure 3-5 shows a plot of the deposition rate as a function of substrate temperature plotted in an Arrhenius form. It can be seen that the deposition rate increases with decreasing substrate temperature. Using the assumption stated previously that the deposition rate is proportional to the overall reaction rate constant, the apparent activation energy from the slope of the linear regression line is found to be -24.6 +/- 1.7 kJ/mol.

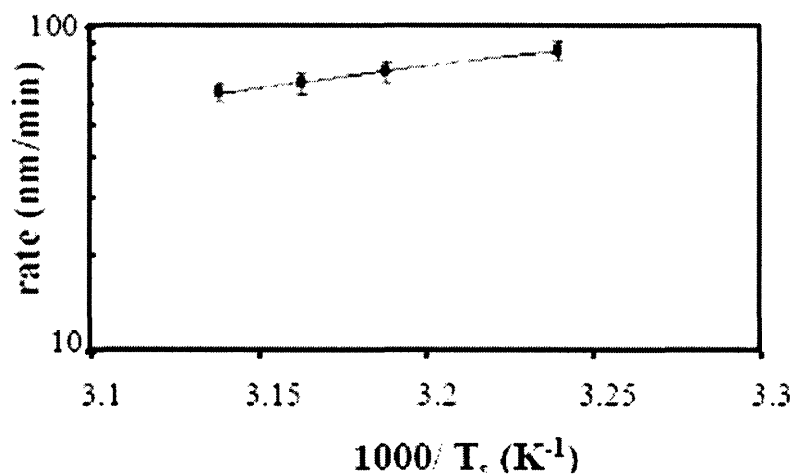


Figure 3-5: Deposition rate as a function of the substrate temperature plotted in an Arrhenius form. The filament temperature is held constant at 245 °C.

Gel permeation chromatography was used to find the number-average molecular weights, M_n , of the films shown in Figure 3-5. This data is plotted in an Arrhenius form in Figure 3-6. It can be seen that the number-average molecular weight also increases with decreasing substrate temperature and the apparent activation energy from the slope of the linear regression line is -22.4 ± 1.4 kJ/mol. The exponential increase of both the deposition rate and the number-average molecular weight with decreasing substrate temperature has been seen in the iCVD polymerization of ethyl acrylate, glycidyl methacrylate, and cyclohexyl methacrylate in the small-scale reactors [25,26]. In those studies, a quartz-crystal microbalance was used to show that decreasing the substrate temperature increases the monomer surface concentration. A kinetic model was then used to show that both the rate of polymerization and the chain length are directly proportional to the monomer surface concentration and therefore both the deposition rate and the molecular weight increase with decreasing substrate temperature.

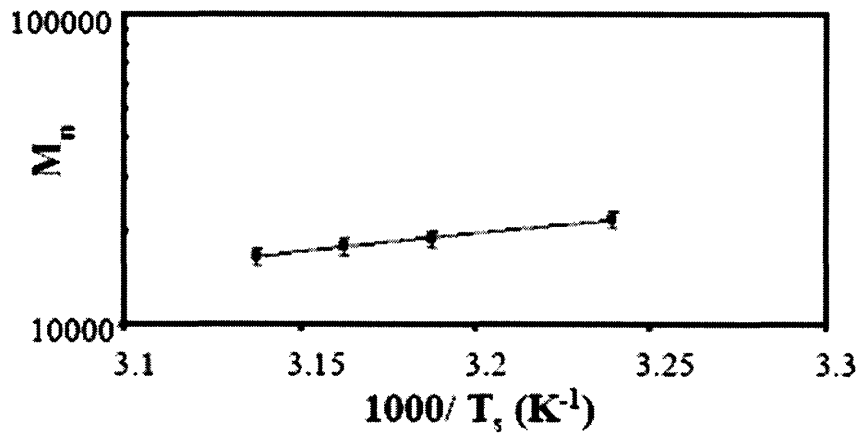


Figure 3-6: Number-average molecular weight, M_n , as a function of substrate temperature plotted in an Arrhenius form. The filament temperature is held constant at 245 °C.

Fourier transform infrared spectroscopy (FTIR) was used to verify whether the epoxide functionality of PGMA films was retained during the iCVD process in the roll-to-roll reactor. Figure 3-7 compares the FTIR spectra of the iCVD PGMA films at different deposition temperatures to the FTIR spectrum of conventionally polymerized PGMA. The epoxide group has characteristic absorption bands at 907, 848, and 760 cm^{-1} [27]. It is seen that the epoxide functionality is retained at the various deposition conditions and there is good agreement between the chemical structure of the iCVD PGMA films and conventionally polymerized PGMA film.

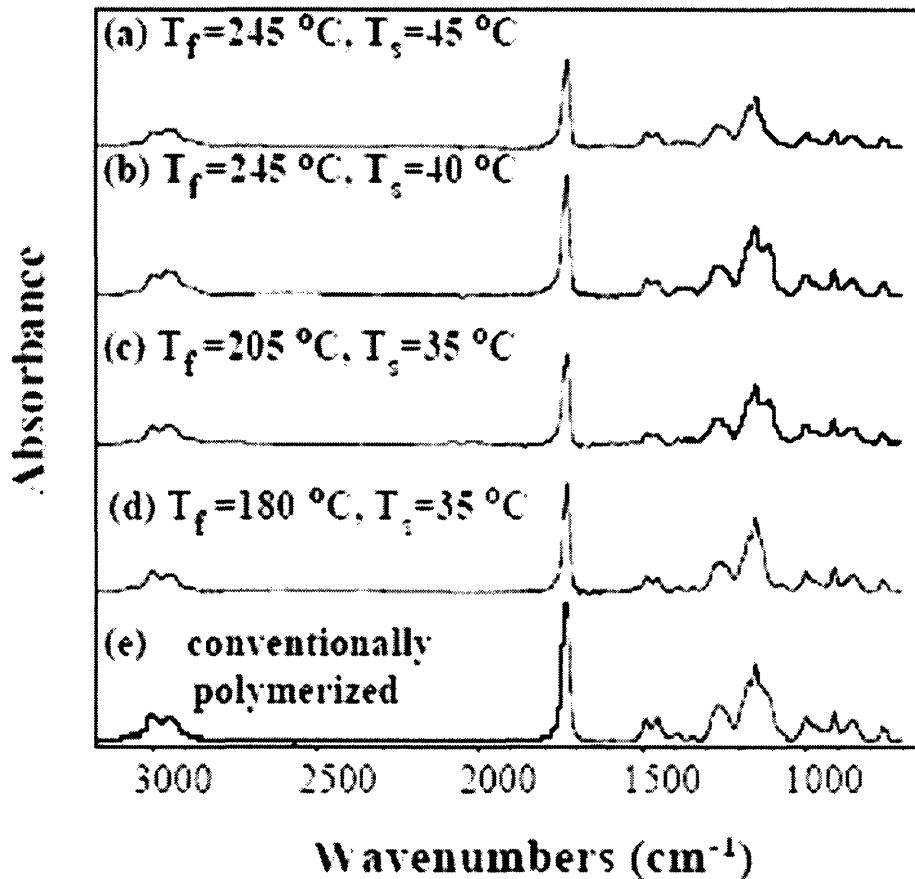


Figure 3-7: FTIR spectra of PGMA films deposited at various filament and substrate temperatures and the FTIR spectrum of conventionally polymerized PGMA. The epoxide group has absorption bands at 907, 848, and 760 cm^{-1} .

3.4.3 Moving Substrate

Stationary wafers were placed along the entire width and height of the coating zone in order to verify the uniformity along both directions. Figure 3-8 shows a plot of the thickness in both the x- and y-directions for a film deposited at a filament temperature of 245° and a substrate temperature of 35° for 10 minutes. The average thickness in the x-

direction is $925 \text{ nm} \pm 73 \text{ nm}$ and the average thickness in the y-direction $862 \text{ nm} \pm 49 \text{ nm}$. During the rolling processes, the deviations in the y-direction will average out.

The deposition rate on a moving substrate was measured by attaching a small piece of silicon substrate to a flexible plastic film that was wound tightly around the rolls. Since the plastic film prevents the moving substrates from directly contacting the heat exchanger, the moving substrates are warmer than the stationary substrates that were in direct contact with the heat exchanger. In order to compare the deposition rates on stationary and moving substrates at the same substrate temperature, the plastic film was placed between a stationary substrate and the heat exchanger and the stationary deposition rate was found to be 24 nm/min . This rate is significantly lower than the deposition rate if there were no plastic film between the substrate and the heat exchanger (68 nm/min). It is hypothesized that the plastic film barrier causes the substrate to be warmer which causes a lower deposition rate as explained earlier through Figure 3-5.

In order to measure the deposition rate on a moving substrate, the substrate was moved from the top of the coating zone to the bottom of the coating zone at speeds ranging from 20 mm/min and 60 mm/min . The amount of time that the substrate spends in the coating zone is inversely proportional to the speed of the substrate. If L is the length of the coating zone, then the total film thickness on the substrate is:

$$thickness = \frac{L}{substrate\ velocity} \times deposition\ rate \quad (4)$$

If the deposition rate is a constant that does not change with substrate velocity, then a plot of film thickness versus the inverse of the substrate velocity should yield a straight line.

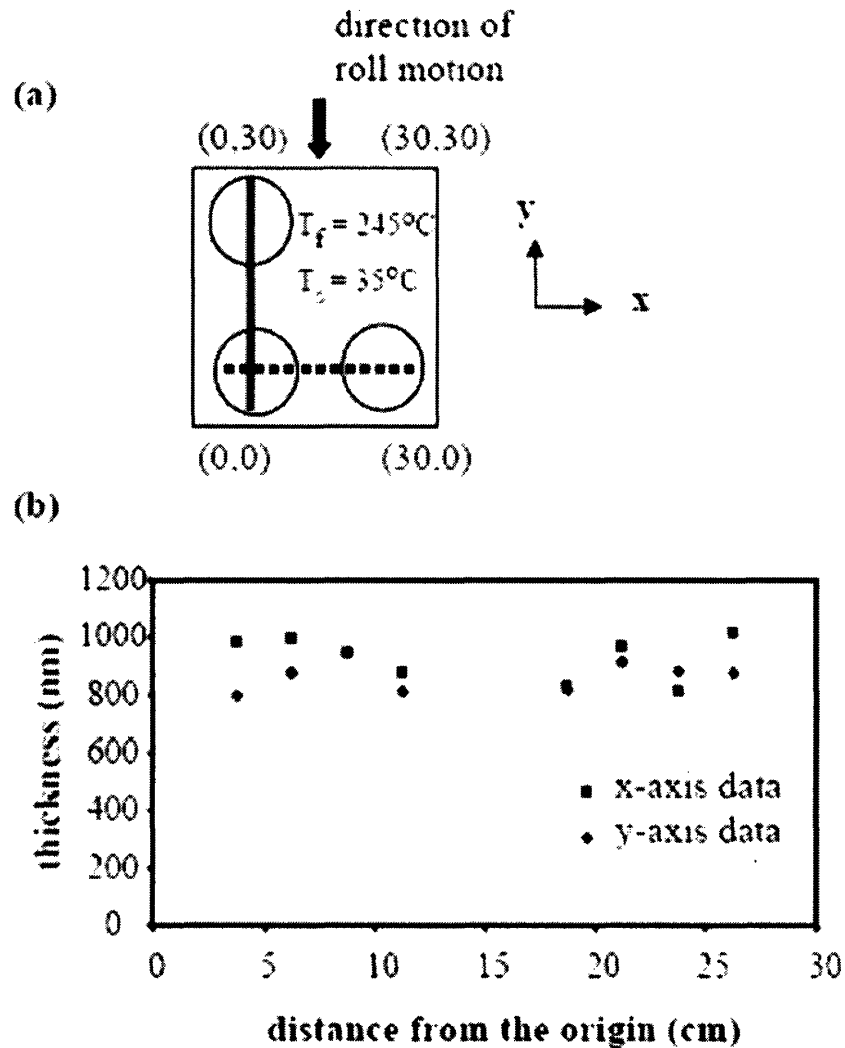


Figure 3-8: Thickness uniformity of PGMA films deposited at a filament temperature of 245° and a substrate temperature of 35° for 10 minutes. (a) Placement of wafers along the cooling stage. (b) Plot showing thickness uniformity along both the x- and y- directions.

Figure 3-9 shows the film thickness versus the inverse of the substrate velocity. The solid squares represent the data for the moving substrate. The dashed line represents equation (4) with the deposition rate equal to the stationary deposition rate (24 nm/min). It can be seen that the moving substrate data falls along the dashed line indicating that the

moving deposition rate is equal to the stationary deposition rate to within experimental error. This is to be expected since at these substrate speeds, the gas velocity is 20 to 50 times faster than the substrate velocity. The moving substrate is therefore stationary relative to the gas flow and therefore does not significantly change the flow profile. The transport processes for the stationary substrate and the moving substrate are therefore similar and the deposition rate remains the same.

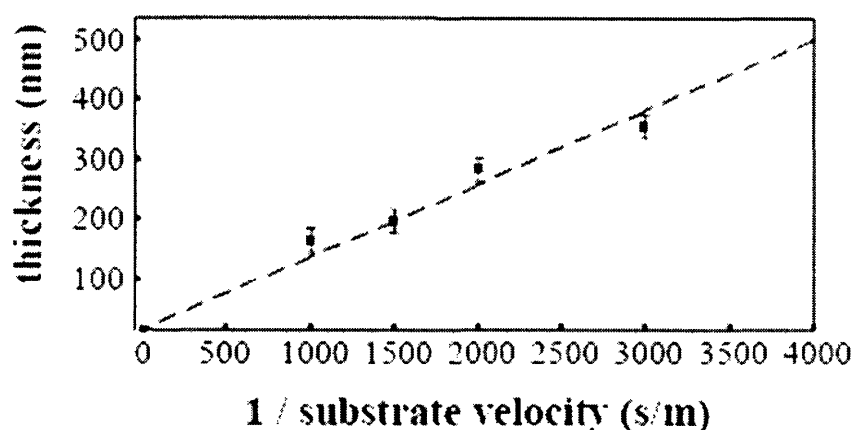


Figure 3-9: Thickness as a function of the inverse of the substrate velocity. The solid squares represent the data for the moving substrate and the dashed line represents the data for the stationary substrate.

3.5 Conclusions

The iCVD polymerization of glycidyl methacrylate was scaled up in a custom modified roll-to-roll reactor. A deposition rate as high as 85 nm/min was achieved on a large 12 inch by 12 inch area. The deposition rate was shown to increase with increasing filament temperature. Both the deposition rate and the number-average molecular weight were found to increase with decreasing substrate temperature. FTIR showed that the epoxide functionality of the PGMA films was retained during the iCVD process. The substrate was moved through the reaction zone at speeds between 20 mm/min and 60

mm/min. At these speeds, the deposition rate on the moving substrate was found to be equal to the deposition rate on the stationary substrate.

3.6 Acknowledgments

This research was supported in part by the U.S. Army through the Institute for Soldier Nanotechnologies, under contract DAAD-19-02-D-0002, with the U.S. Army Research Office. The content does not necessarily reflect the position of the government, and no official endorsement should be inferred.

3.7 References

- [1] M. Iijima, Y. Takahashi, *Macromolecules* 22 (1989) 2944.
- [2] M. Tamada, H. Omichi, N. Okui, *Thin Solid Film* 268 (1995) 18.
- [3] J.R. Salem, F.O. Sequeda, J. Duran, W.Y. Lee, *J. Vac. Sci. Technol. A* 4 (1986) 369.
- [4] C.C. Roberts, G.-R. Yang, A. Coccoziello, Y.-P. Zhao, G. Wnek, T.-M. Lu, *Appl. Phys. Lett.* 68 (1996) 2067.
- [5] J. Lin, S.K. Murthy, B.D. Olsen, K.K. Gleason, A.M. Klibanov, *Biotechnology Letters* 25 (2003) 1661.
- [6] S.J. Limb, K.K. Gleason, D.J. Edell, E.F. Gleason, *J. Vac. Sci. Technol. A* 15 (1997) 1814.
- [7] K. Chan, K.K. Gleason, *Chem. Vap. Deposition* 11 (2005) 437.
- [8] Y. Mao, K.K. Gleason, *Langmuir* 20 (2004) 2484.
- [9] K. Chan and K.K. Gleason, *Langmuir* 21 (2005) 8930.
- [10] M. Ma, Y. Mao, M. Gupta, K.K. Gleason, G.C. Rutledge, *Macromolecules* 38 (2005) 9742.
- [11] Y. Mao, K.K. Gleason, *Macromolecules* (to be published).
- [12] M. Izu, S. Ovshinsky, *Thin Solid Films* 119 (1984) 55.
- [13] R.E.I. Schropp and M. Zeman, *IEEE Trans. Electron Dev.* 46 (1999) 2086.
- [14] J. Rudiger, H. Brechtel, A. Kottwitz, J. Kuske, U. Stephan, *Thin Solid Films* 427 (2003) 16.
- [15] A. Ledermann, U. Weber, C. Mukherjee, B. Schroeder, *Thin Solid Films* 395 (2001) 61.
- [16] G. Voorwinden, R. Kniese, M. Powalla, *Thin Solid Films* 431-432 (2003) 538.
- [17] S. Boughaba, G.I. Sproule, J.P. McCaffrey, M. Islam, M.J. Graham, *Thin Solid Films* 358 (2000) 104.
- [18] M. Kim, S. Kiyohara, S. Konishi, S. Tsuneda, K. Saito, T. Sugo, *J. Membr. Sci.* 117 (1996) 33.

-
- [19] C.A. Orr, J.J. Cernohous, P. Guegan, A. Hirao, H.K. Jeon, C.W. Macosko, *Polymer* 42 (2001) 8171.
- [20] A. Argoitia, C.S. Kovach, J.C. Angus, in: M.A. Prelas, G. Popovici, L.K. Bigelow (Eds.), *Handbook of Industrial Diamonds and Diamond Films*, Marcel Dekker, Inc., New York, 1998.
- [21] R.B. Bird, W.E. Stewart, E.N. Lightfoot, *Transport Phenomena*, John Wiley & Sons, New York, 2002.
- [22] W.M. Deen, *Analysis of Transport Phenomena*, Oxford University Press, New York, 1998.
- [23] Y. Mao, K.K. Gleason, *Langmuir* 20 (2004) 2484.
- [24] E.R.G. Eckert, R.M. Drake, Jr., *Analysis of Heat and Mass Transfer*, McGraw-Hill Book Company, New York, 1972.
- [25] K.K.S. Lau, K.K. Gleason, *Macromolecules* (to be published).
- [26] K. Chan, K.K. Gleason, *Macromolecules* (to be published).
- [27] D. Lin-Vien, N.B. Colthup, W.G. Fateley, J.G. Grasselli, *The Handbook of Infrared and Raman Characteristic Frequencies of Organic Molecules*, Academic Press, Inc., Boston, 1991.

Chapter Four:

Surface Modification of High Aspect Ratio

Surface Modification of High Aspect Ratio Pores

and Surface Features by initiated Chemical Vapor

Deposition (iCVD)

Malancha Gupta, Vivek Kapur, Nathalie Pinkerton, and Karen K. Gleason. "Surface Modification of High Aspect Ratio Surface Modification of High Aspect Ratio Pores and Surface Features by initiated Chemical Vapor Deposition (iCVD)", submitted.

4.1 Abstract

The initiated chemical vapor deposition (iCVD) technique was used to modify the internal surfaces of polymeric capillary pore membranes with a thin layer of poly(1H,1H,2H,2H-perfluorodecyl acrylate) coating in order to make water-repellant, self-cleaning membranes. X-ray photoelectron microscopy data confirmed the presence of coating on the topside and the backside of the membranes and electron microprobe analysis confirmed the presence of the coating along the internal pore wall. Static and dynamic contact angle measurements (low hysteresis) showed that the coated membranes were hydrophobic. It was found that the iCVD process can be used to coat pores with aspect ratios as high as 80:1. The ability to coat high aspect ratio trenches in silicon wafers was also demonstrated.

4.2 Introduction

The surface modification of high aspect ratio microstructures has applications in several fields such as biology, textiles, and microelectronics. Silicon membranes have been functionalized with biotin in order to create membranes that can selectively capture biological organisms.¹ Atomic layer deposition was used to conformally coat silicon trenches for microelectronic applications.² Plasma polymerization was used to coat silicon trenches to make non-adhesive silicon molds for soft lithography.³ Plasma-induced grafting has been used to attach hydrophilic polymers onto the surfaces of hydrophobic membranes in order to prevent membrane fouling caused by protein adsorption.^{4,5}

iCVD is a one-step, low energy process (0.01 W/cm^2) that can be used to produce polymeric thin films in which the pendant chemical moieties are kept intact.⁶ This all-dry process has environmental benefits because no solvents are used. The iCVD process can be used to conformally coat small features such as carbon nanotube forests⁷ and particles⁸ since the surface tension problems associated with liquids are not present. The iCVD technique has been used to polymerize a wide variety of vinyl monomers such as glycidyl methacrylate⁹ and 2-hydroxyethyl methacrylate.¹⁰ The proposed polymerization mechanism is the classical free radical polymerization mechanism of vinyl monomers. Monomer and initiator gases are fed into a vacuum chamber where resistively heated wires are used to thermally decompose the initiator molecules into free radicals. Tert-butyl peroxide is commonly used as the initiator. The initiator radicals then diffuse to the substrate and adsorb onto the surface. The substrate temperature is kept cool to promote the adsorption of the free radicals as well as the monomer molecules. The initiation,

propagation, and termination events occur on the surface of the cooled substrate to form a polymer film. The deposition rates achieved in the iCVD process (~200 nm/min) are an order of magnitude higher than the deposition rates achieved in pulsed plasma polymerization.¹¹ The slow deposition rates in plasma polymerization are due to the complexity of the plasma process. The high energy of the plasma partially breaks the monomer and there is also a competition between etching and deposition. The iCVD process only breaks the initiator and leaves the monomer completely intact.

Low surface energy polymeric coatings have many uses due to their hydrophobic and oleophobic properties.^{12,13} In our previous study,¹¹ iCVD was used to polymerize the 1H,1H,2H,2H-perfluorodecyl acrylate (PFDA, $\text{CH}_2=\text{CHCOOCH}_2\text{CH}_2(\text{CF}_2)_7\text{CF}_3$) at deposition rates as high as 375 nm/min. The poly(1H,1H,2H,2H-perfluorodecyl acrylate) (PPFDA) thin films have a lower surface energy (9.3 mN/m) than poly(tetrafluoroethylene) (18 mN/m) because PFDA contains CF_3 end groups.^{14,15} The static contact angle on the PPFDA thin films was found to be $120.8^\circ \pm 1.2^\circ$, which is the maximum contact angle that can be achieved on a flat hydrophobic surface.¹⁶ Fourier transform infrared spectroscopy and x-ray photoelectron spectroscopy showed full retention of the fluorine moieties and no measurable crosslinking was detected. Gel permeation chromatography experiments showed that high molecular weight films (~100,000 g/mol) were made.

The goal of this study is to use the iCVD technique to functionalize capillary pore polymeric membranes with PPFDA in order to make water-repellant, self-cleaning membranes. The iCVD process has already been used to coat electrospun fiber mats with PPFDA, but the disordered arrangement of fibers produces tortuous pores of ill defined

length and diameter.^{17,18} In contrast, the capillary pore membranes used in this study have cylindrical pores of well-defined diameter which form ordered arrays. The capillary pore membrane geometry can be systematically varied (pore diameter, pore length, and degree of porosity), enabling fundamental examination of the iCVD process for coating features with different aspect ratios (ratio between length and diameter).

The capillary pore membranes used in this study have a pore diameter of 3 microns and pore lengths of either 120 microns or 240 microns corresponding to aspect ratios of 40:1 and 80:1 respectively. The nominal porosity of the membranes is either 30% or 50%. Figure 4-1 shows scanning electron microscope (SEM) images of a capillary pore membrane with an aspect ratio of 80:1. It can be seen that the pore size is uniform. The membranes were immersed in liquid nitrogen and then cracked in order to visualize the cross section (Figure 4-1b).

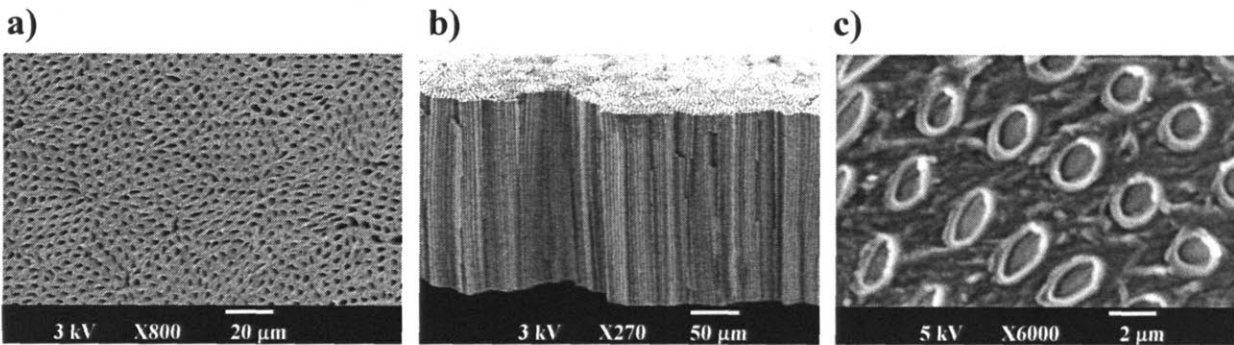


Figure 4-1: a) Topdown and b) cross section SEM micrographs of a 240 μm thick capillary pore membrane. The average pore diameter is 3 μm and the nominal porosity is 50%. c) Enlarged image of a membrane with a nominal porosity of 30%.

4.3 Experimental Methods

1H,1H,2H,2H-Perfluorodecyl acrylate (PFDA) monomer (97%, Aldrich) and tert-butyl peroxide initiator (98%, Aldrich) were used without further purification. The iCVD polymerization was conducted in a custom-built cylindrical reactor (240 mm diameter, 33 mm height). The PFDA monomer was heated to 80°C and fed into the chamber at a flowrate of 0.3 sccm through a heated mass flow controller (Model 1152C, MKS) and the initiator was kept at room temperature and fed into the chamber at a flowrate of 0.7 sccm through another mass flow controller (Model 1479A, MKS). The reactor pressure was kept constant at 100 mTorr. Nichrome filaments (80% Ni/20% Cr) were resistively heated to 300°C. The distance between the filaments and the substrate was kept at 29 mm. The membranes substrates were taped down on all four sides onto a stage that was backside cooled at a constant temperature of 44°C using water from a recirculating chiller. The capillary pore membranes used in this work were fabricated at DuPont using a proprietary process. The membranes were made of a copolymer of ethylene (88 weight %) and methacrylic acid (12 weight %) and had a pore diameter of 3 microns and pore lengths of either 120 microns or 240 microns. The nominal porosity of the membranes was either 30% or 50%. Silicon trenches (3µm width, 6 µm depth, 8 µm spacing between trenches) were coated with a thick layer of PPFDA (520 nm) in order to visualize the coating along the trench walls. Silicon trenches (1µm width, 6 µm height, 8 µm spacing between trenches) were coated with 1500 nm of PPFDA in order to completely fill the trenches.

X-ray photoelectron microscopy (XPS) (Kratos AXIS Ultra spectrometer with a monochromatized Al K α source) and electron microprobe analysis (EMPA) (JEOL JXA-

733 Superprobe) were used to study the chemical composition of the membranes. Contact angle measurements were conducted using a goniometer (Ramé-Hart Model 500). Scanning electron microscopy (SEM) (JEOL 6060) was used to image the membranes. A quartz crystal microbalance (QCM) (Sycon Instruments) with a 16 mm diameter gold-coated crystal sensor was used to conduct adsorption measurements. The QCM was placed inside the reactor chamber and was kept at a constant temperature of 44°C using a chiller. The initiator flow was replaced with nitrogen and the filaments were kept off. In each run, monomer and nitrogen were flowed into the reactor and the pressure was increased to the reaction pressure (100 mTorr) and the adsorbed monomer volume was recorded. It can be assumed that these are equilibrium measurements since sufficient time was allowed for the QCM to stabilize to a constant value. A capillary flow porometer (Porous Media Inc.) was used to conduct hydrohead tests on the coated membranes. Approximately 5 ml of distilled and deionized water was laid over one surface of the membrane in order to create a small pool of liquid that completely covered the surface of membrane. The membrane was then subjected to a slowly increasing pressure provided by a nitrogen head. The pressure at which gas flow rate was first observed was used to estimate the water breakthrough pressure of the largest pore in the membrane sample.

4.4 Results and Discussion

In order to study whether the initiator and monomer molecules are able to infiltrate these high aspect ratio pores during the coating process, the change in contact angle of the topside and backside of the membrane after coating was monitored (Figure 4-2a). Since the membranes were taped down to the cooling stage on all four sides, the only possible method for the backside of the membrane to become coated with PPFDA

would be if the reactants traveled through the pores. A non-porous membrane was used to verify the absence of diffusion under the edges of the taped sample. This control non-porous membrane had a contact angle of 79° before coating. After coating, the topside of the non-porous substrate had a contact angle of 121° while the bottom of the substrate still had a low contact angle of 81° , confirming that as expected, coating of the backside did not occur. Subsequently, 30% and 50% porous membranes of aspect ratio 80:1 were taped down and coated. Before coating, the 30% porous membrane had a contact angle of 87° . After coating, both the topside and backside contact angles increased to 135° and 137° respectively. Before coating, the 50% porous membrane had a contact angle of 105° . After coating, both the topside and backside contact angles increased to 151° and 152° respectively. Since the backside of the porous membranes were coated, it can be concluded that diffusion of species through the pores enables the iCVD process to coat features having aspect ratios of at least 80:1.

The contact angle measurements in Figure 4-2a indicate that the hydrophobicity increases with porosity. The hydrophobicity of a flat substrate can be increased either by lowering the surface energy through a change in surface chemistry or by adding roughness to the surface.^{19,20} It has been found that the maximum contact angle that can be achieved on a flat surface using surface chemistry alone is 120° ²¹ and static contact angles higher than 120° can only be achieved through the addition of surface roughness. A rough, hydrophobic surface can exist in two different states: Wenzel or Cassie-Baxter. In the Wenzel state,²² the water droplet penetrates the pore and there is a large hysteresis between advancing and receding contact angles. In the Cassie-Baxter state,²³ the water droplet does not penetrate the pore and instead sits on top of the pores. There is low

hysteresis in the Cassie-Baxter state. For practical applications that require hydrophobicity, water droplets should not penetrate the pores and therefore the Cassie-Baxter state is required. In the Cassie-Baxter model, the apparent contact angle, θ^* , is $\cos \theta^* = \phi_s \cos \theta - \phi_v$, where θ is the contact angle on a flat surface (120° for PPFDA coated surfaces) and ϕ_s and ϕ_v are the solid-liquid and air-liquid contact area per unit projected surface area respectively. In order to calculate ϕ_s and ϕ_v for the membranes, a geometric model was made for both the 30% and 50% porous substrates in which the pores were assumed to be arranged in a square array. The pores were represented as circles with radius r and the distance between the centers of two adjacent pores was $2r+2s$. The Cassie-Baxter equation for the membranes using this geometric model is:

$$\cos \theta^* = \frac{(2r+2s)^2 - \pi r^2}{(2r+2s)^2} \cos \theta - \frac{\pi r^2}{(2r+2s)^2} \quad (1)$$

Figure 4-2b shows a plot that compares the theoretical contact angles calculated using equation 1 with the experimentally measured contact angles. Both the theoretical results and the experimental results show the same trend of increasing contact angle with increased porosity. The theoretical results, however, underestimate the experimental results. This discrepancy is due to the fact that the processing method used to make the capillary pore membranes adds another level of roughness to the membrane surface that is not accounted for in equation 1. For example, the SEM image in Figure 4-1c shows protrusions on the surface regions in between the pores.

a)

	0% porosity	30% porosity	50% porosity
no coating	 79°	 87°	 105°
top side	 121°	 135°	 151°
bottom side	 81°	 137°	 152°

b)

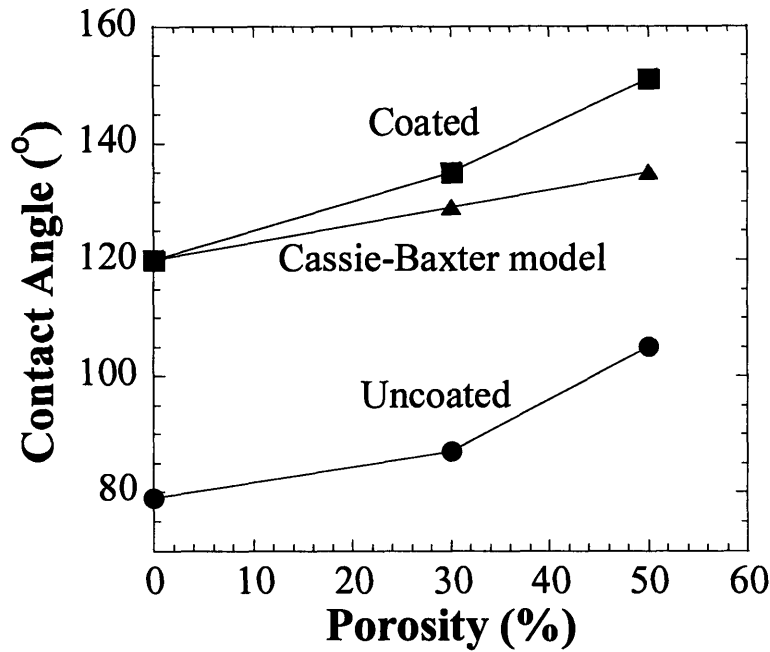


Figure 4-2: a) Measured static contact angles for uncoated and coated membranes (topside and backside). b) Comparison of the experimental contact angles for uncoated (circles) and coated membranes (squares) and the contact angles predicted using the Cassie-Baxter model (triangles). The Cassie-Baxter model predicts the correct trend but underestimates the experimental values.

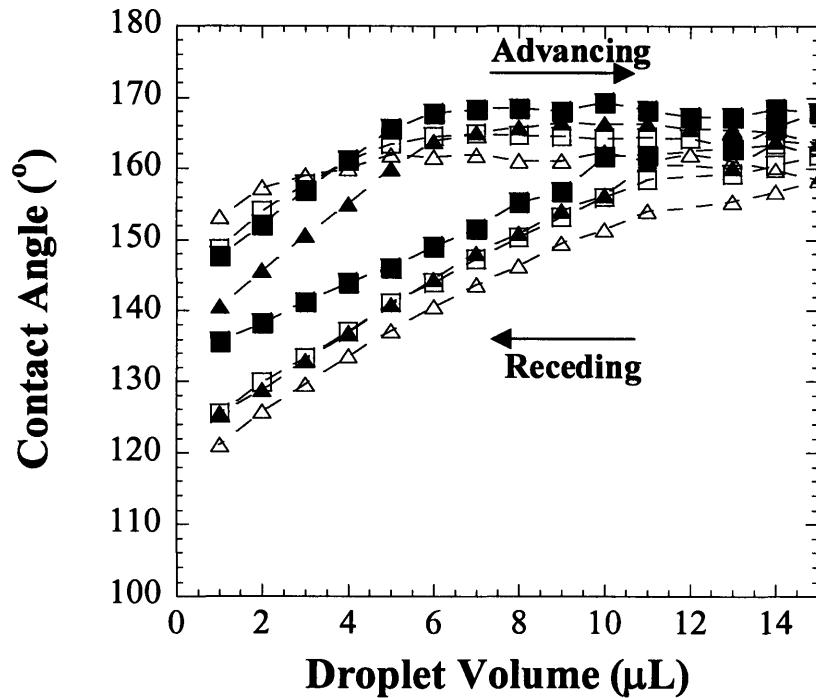


Figure 4-3: Advancing and receding contact angle measurements for 50% porous membranes with pore lengths of 120 microns (unfilled) and 240 microns (filled). The measurements were taken from the topside (triangles) and the bottom side (squares). The low hysteresis measured on both sides confirms that coating has been achieved along the entire length of the inner pore wall.

Figure 4-3 shows the advancing and receding contact angles measured on both the topside and the backside of membranes having pores with aspect ratios of 40:1 and 80:1. The low hysteresis verifies that the membranes are indeed in the Cassie-Baxter state. The low hysteresis implies that the inner pore walls of the membrane are coated during the iCVD process. If the inner pore walls had not been coated, the measured hysteresis would be much higher since the droplet would penetrate the pore during the receding measurements (Wenzel state). The hydrophobic coating along the pore walls prevents the water from penetrating the pore. Figure 4-3 shows no measurable difference between the

contact angles measured from the topside and the backside of the membranes. This indicates that the coating is present along the entire length of the pore walls.

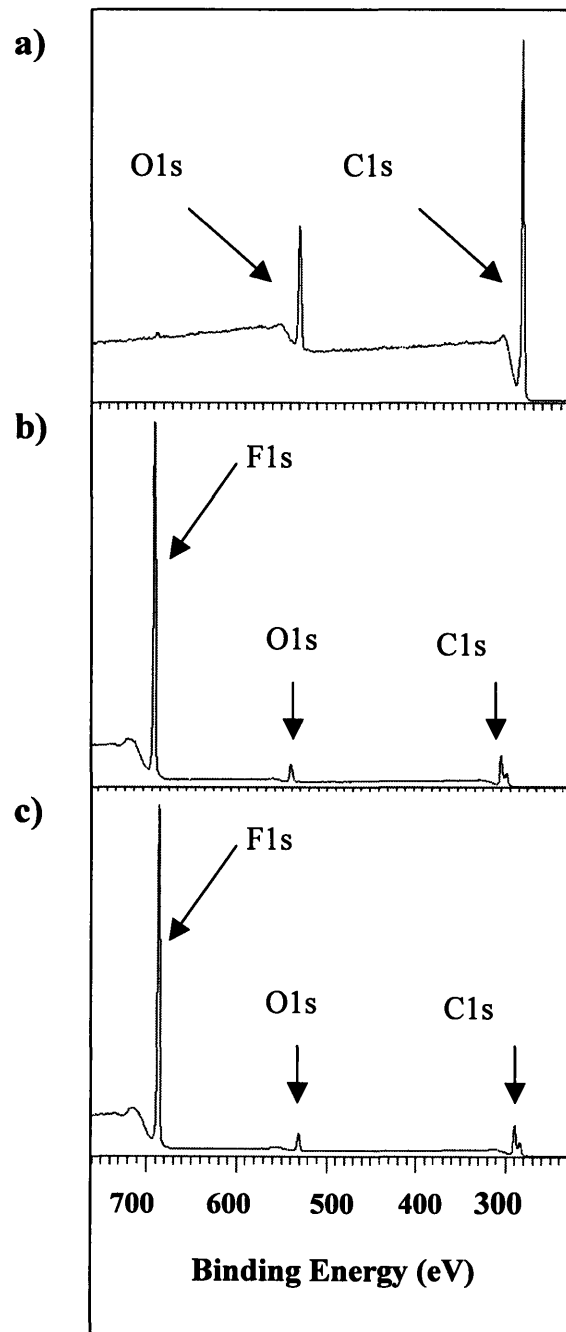


Figure 4-4: XPS survey scans for detection of the atomic concentration of fluorine, oxygen, and carbon in a) the uncoated membrane, b) the topside of the coated membrane, and c) the backside of the coated membrane.

Figure 4-4 shows the X-ray photoelectron microscopy (XPS) survey scans of the uncoated membrane, the topside of the coated membrane, and the backside of the coated membrane. Since the capillary pore membrane is made of a copolymer of ethylene and methacrylic acid, the spectrum of the uncoated membrane contains only carbon and oxygen peaks. The coated sample contains fluorine peaks in both the topside and backside spectra confirming the presence of coating on both sides of the membranes. The atomic percentages calculated on a hydrogen free basis from the survey scans are 42.9% carbon, 4.2% oxygen, and 52.9% fluorine for the topside and 43.8% carbon, 4.2% oxygen, and 52.0% fluorine for the backside. These values are in reasonable agreement with the theoretical values calculated using the chemical formula of the PFDFA monomer (40.6% carbon, 6.3% oxygen, and 53.1% fluorine). Since the XPS sampling depth is approximately 5 nm,²⁴ the agreement between the theoretical and experimental atomic concentrations indicate that at least 5 nm of PPFDA coating is present.

Table 4-1. Weight Gain and Calculated Thickness After 5 and 10 Minutes of iCVD PPFDA Coating

		5 minutes of coating		10 minutes of coating	
volume % porosity	pore length (μm)	weight/area (g/cm ²)	thickness (nm)	weight/area (g/cm ²)	thickness (nm)
0	NA	0.007	72	0.014	138
30	120	0.080	18	0.187	43
30	240	0.146	16	0.269	30
50	240	0.176	14	0.324	25

The membranes were weighed before and after coating in order to determine the amount of PPFDA coating as a function of pore length and porosity. Table 4-1 shows the weight gain per square area of membrane after 5 minutes of coating and after 10 minutes of coating. Table 4-1 shows the following trends: the porous membranes gain more than

10 times more coating per unit area than the nonporous membranes, increasing the pore length from 120 μm to 240 μm roughly doubles the amount of weight gain, and increasing the porosity from 30% to 50% increases the weight gain. These effects are caused by the fact that the pores introduce additional internal surface area on which the iCVD polymerization of PFDA can occur and therefore there is more coating per square area of membrane if the pore length or porosity is increased. The thickness of the PPFDA coating on the membrane was calculated by first dividing the weight gain by the density of the polymer film, which is assumed to be 1 g/cm^3 , and then correcting for the surface area introduced by the pores. The assumption used in the calculation is that the film coverage is uniform. Table 4-1 shows that doubling the deposition time roughly doubles the thickness of the coating. All of the calculated thicknesses are indeed greater than 5 nm, as expected from the XPS results.

While the ability of the iCVD process to coat the internal pore surfaces of the membranes can be inferred from all the previous results, direct confirmation of the presence of fluorine along the pore wall was obtained by electron microprobe analysis (EMPA). As shown in Figure 4-1b, cross sections of the membranes were made by freezing with liquid nitrogen and then cracking. Then the EMPA beam (spot size of 1 μm diameter and 1 μm depth) was rastered along the entire length of a single pore in 20 μm increments. Figure 4-5 shows the fluorine signal detected by EMPA as a function of the distance along the pore wall for membranes that were coated for 2 minutes and membranes that were coated for 5 minutes. The data confirms the presence of iCVD PPFDA along the entire length of both the 40:1 and 80:1 aspect ratio pores. From weight measurements, the thickness of the PPFDA coating on the membranes was estimated to

be 6 nm and 15 nm after coating for 2 minutes and 5 minutes respectively. As expected, the membranes with 15 nm coating show a higher fluorine signal than those with only 6 nm of coating. Figure 4-5 shows a higher fluorine signal at the entrance of the pore wall than at the exit for all membranes. The fluorine signal levels off to a constant value after approximately 50 μm along the pore wall. In terms of coating thickness, the decreasing fluorine signal in Figure 4-5 implies that the coating thickness at the entrance is approximately 10 nm more than the coating at the exit. Since the pore diameter (3 μm) is two orders of magnitude larger than the coating thickness at any point along the pore wall, the coating is relatively uniform throughout the pore.

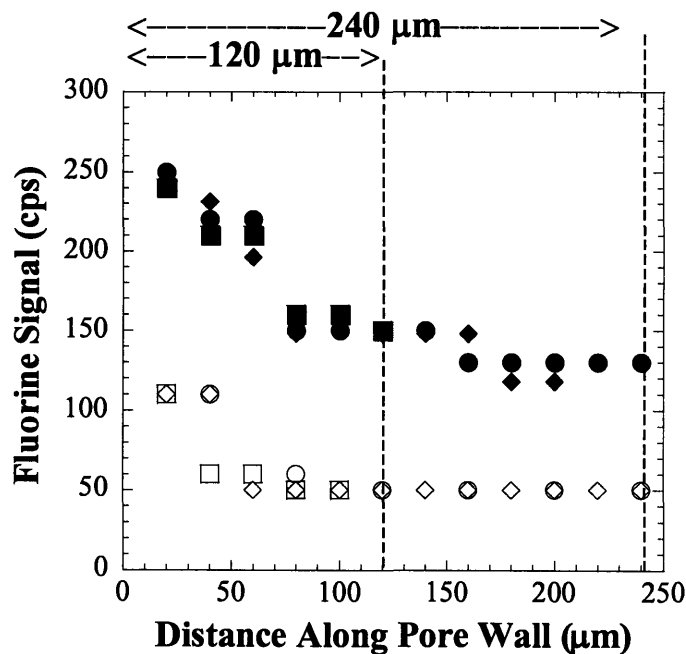


Figure 4-5. Electron microprobe data for membranes coated for 2 minutes (unfilled) and 5 minutes (filled). Three different membranes were employed: 30% porosity and 120 μm length (squares), 30% porosity and 240 μm length (circles), and 50% porosity and 240 μm length (diamonds). The average pore diameter for all the membranes was 3 μm .

In order to investigate the mechanism that allows the PPFDA coating to be relatively uniform within high aspect ratio pores, the sticking coefficient was measured. The sticking coefficient is defined as the ratio of the number of molecules that adsorb on the surface to the total number of molecules that impinge on the surface.^{25,26} The sticking coefficient can be estimated using the film deposition rate and the monomer flux²⁷ and is found to be approximately 1×10^{-6} . This low sticking coefficient is typical of fluorinated molecules²⁷ and is the reason that the PPFDA coating is quite uniform throughout these high aspect ratio pores. If the sticking coefficient had been closer to unity, the monomer would have stuck to the top surface and would not have infiltrated the pores. Figure 4-6 shows SEM images of silicon trenches coated with PPFDA using the iCVD technique. The uniformity of the coating along the trench walls can be visually seen (Figures 4-6a and 4-6b). The ability to create a vertical seam and thus completely fill the trench with PPFDA is shown in Figure 4-6c.

For practical applications, hydrophobic membranes should have a high breakthrough pressure. The breakthrough pressure is the pressure at which the water first breaks through the pores. In order to measure this pressure, the dry PPFDA coated membrane was brought in contact with water and an increasing pressure was applied to the water until the first drop of water appeared on the other side of the membrane. The Laplace-Young equation²⁸ predicts that the breakthrough pressure is inversely proportional to the diameter of the pore. The breakthrough pressures of PPFDA coated membranes with pore diameters of 3 μm and 10 μm were tested and were found to be as high as 8.3 psi and 2.2 psi respectively. These values match those predicted by the Laplace-Young equation for hydrophobic membranes (7 psi and 2 psi respectively). Thus

the PPFDA coated capillary pore membranes meet the requirement of having a high breakthrough pressure and further improvements are predicted as pore diameter decreases.

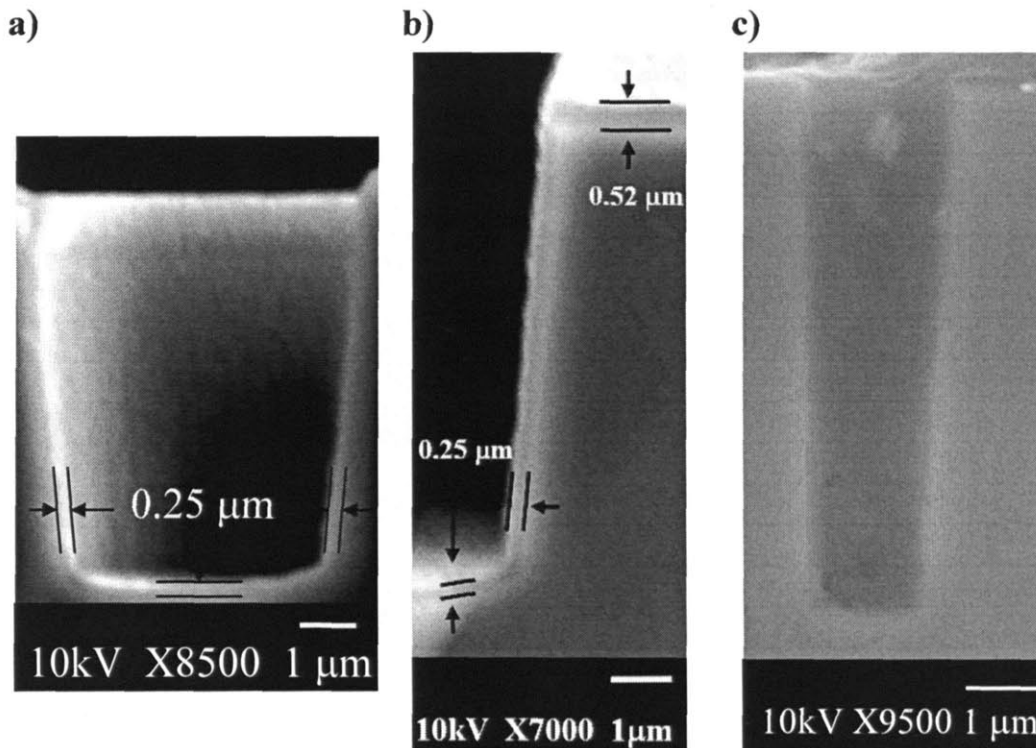


Figure 4-6: a) SEM cross-sectional micrograph of a silicon trench (3 μ m width, 6 μ m depth) conformally coated by a 0.25 μ m thick layer of iCVD PPFDA. b) Enlarged image of the right side of the trench. c) A silicon trench (1 μ m width, 6 μ m depth) completely filled with a thick layer of iCVD PPFDA.

4.5 Conclusion

In conclusion, the iCVD process can be used to functionalize membranes with high aspect ratio (\sim 80:1) pores. X-ray photoelectron microscopy data confirmed the presence of the PPFDA coating on the topside and the backside of the membranes and electron microprobe analysis confirmed the presence of the coating along the pore wall. Static and dynamic contact angle measurements (low hysteresis) showed that the coated

membranes exist in the Cassie-Baxter state. The low sticking coefficient of the PFDA monomer ($\sim 10^{-6}$) allows the PPFDA coating to be quite uniform throughout these high aspect ratio pores. Future work will include using the iCVD process to functionalize capillary pore membrane surfaces with other acrylate polymers.

4.6 Acknowledgments

We would like to thank our DuPont collaborator Dr. Vivek Kapur and our undergraduate researcher Natalie Pinkerton. We thank the DuPont MIT Alliance for financial support. We would also like to thank the MIT CMSE shared facilities supported in part by the MRSEC program of the National Science Foundation under award number DMR 02-13282. We would like to thank Dr. Nilanjan Chatterjee at MIT for assistance with the electron microprobe. We would also like to thank Dr. Edward Gleason of Analog Devices for providing the trench structures.

4.7 References

- [1] S. E. Létant, B. R. Hart, A. W. Van Buuren, L. J. Terminello, *Nat. Mater.* **2003**, *2*, 391.
- [2] R. G. Gordon, D. Hausmann, E. Kim, J. Shepard, *Chem. Vap. Deposition* **2003**, *9*, 73.
- [3] L. P. Yeo, Y. H. Yan, Y. C. Lam, M. B. Chan-Park, *Langmuir* **2006**, *22*, 10196.
- [4] D. S. Wavhal, E. R. Fisher, *Journal of Membrane Science* **2002**, *209*, 255.
- [5] H.-Y. Yu, M.-X. Hu, Z.-K. Xu, *Plasma Process. Polym.* **2005**, *2*, 627.
- [6] Y. Mao, K. K. Gleason, *Langmuir* **2006**, *22*, 1795.
- [7] K. K. S. Lau, J. Bico, K. B. K. Teo, M. Chhowalla, G. A. J. Amaratunga, W. I. Milne, G. H. McKinley, K. K. Gleason, *Nano Lett.* **2003**, *3*, 1701.
- [8] K. K. S. Lau, K. K. Gleason, *Adv. Mater.* **2006**, *18*, 1972.
- [9] Y. Mao, K. K. Gleason, *Langmuir* **2004**, *20*, 2484.
- [10] K. Chan, K. K. Gleason, *Langmuir* **2005**, *21*, 8930.
- [11] M. Gupta, K. K. Gupta, *Langmuir*, **2006**, *22*, 10047.
- [12] L. Feng, S. Li, Y. Li, H. Li, L. Zhang, J. Zhai, Y. Song, B. Liu, L. Jiang, D. Zhu, *Adv. Mater.* **2002**, *14*, 1857.
- [13] W. Chen, A. Y. Fadeev, M. C. Hsieh, D. Oner, J. Youngblood, T. J. McCarthy, *Langmuir* **1999**, *15*, 3395.
- [14] A. F. Thunemann, A. Lieske, B.-R. Paulke, *Adv. Mater.* **1999**, *11*, 321.
- [15] I. J. Park, S. B. Lee, C. K. Choi, K. J. Kim, *Journal of Colloid and Interface Science* **1996**, *181*, 284.
- [16] A. Lafuma, D. Quere, *Nat. Mater.* **2003**, *2*, 457.

-
- [17] M. Ma, Y. Mao, M. Gupta, K. K. Gleason, G. C. Rutledge, *Macromolecules* **2005**, *38*, 9742.
- [18] M. Ma, M. Gupta, Z. Li, L. Zhai, K. K. Gleason, R. E. Cohen, M. F. Rubner, G. C. Rutledge, *Adv. Mater.* In Press.
- [19] X. Feng, L. Jiang, *Adv. Mater.* **2006**, *18*, 3063.
- [20] H. Chen, F. Zhang, S. Fu, X. Duan, *Adv. Mater.* **2006**, *18*, 3089.
- [21] A. Lafuma, D. Quere, *Nat. Mater.* **2003**, *2*, 457.
- [22] R. N. Wenzel, *Ind. Eng. Chem.* **1936**, *28*, 988.
- [23] A. B. D. Cassie, S. Baxter, *Trans. Faraday Soc.* **1944**, *40*, 546.
- [24] C. R. Brundle, C. A. Jr. Evans, S. Wilson, *Encyclopedia of Materials Characterization- Surfaces, Interfaces, Thin Films*, Butterworth-Heinemann, Boston **1992**.
- [25] D. M. Hausmann, E. Kim, J. Becker, R. G. Gordon, *Chem. Mater.* **2002**, *14*, 4350.
- [26] T. B. Tighe, T. A. Daniel, Z. Zhu, S. Uppili, N. Winograd, D. L. Allara, *J. Phys Chem. B* **2005**, *109*, 21006.
- [27] B. A. Cruden, Karen K. Gleason, and Herbert H. Sawin, *J. Vac. Sci. Technol. B* **2002**, *20*, 690.
- [28] P. S. Kumar, J. A. Hogendoorn, P. H. M. Feron, G. F. Versteeg, *Chem. Eng. Sci.* **2002**, *57*, 1639-1651.

Chapter Five:

**Surface Modification of Electrospun Mats by
initiated Chemical Vapor Deposition (iCVD)**

Portions of this work were published in *Macromolecules and Advanced Materials*:

Minglin Ma, Yu Mao, Malancha Gupta, Karen K. Gleason, and Gregory C. Rutledge. "Superhydrophobic fabrics produced by electrospinning and chemical vapor deposition", *Macromolecules*, 38, 9742-9748, 2005.

Minglin Ma, Malancha Gupta, Zhi Li, Lei Zhai, Karen K. Gleason, Robert E. Cohen, Michael F. Rubner, and Gregory C. Rutledge. "Superhydrophobic fabrics produced by electrospinning and chemical vapor deposition", *Advanced Materials*, 19, 255-259, 2007.

5.1 Abstract

The initiated chemical vapor deposition (iCVD) method was combined with the electrospinning method in order to create superhydrophobic mats. In the first study, beaded and non-beaded electrospun poly(caprolactone) (PCL) fiber mats ranging in diameter from 600 nm to 2200 nm were coated with a thin layer of poly(perfluoroalkylethyl methacrylate) (PPFEMA) coating using the iCVD technique. Contact angles as high as 175° and sliding angles as low as 2.5° were obtained for the PPFEMA coated mats. In the second study, porous electrospun poly(methyl methacrylate) mats with $1.7\ \mu\text{m}$ fiber diameters and 80 nm pore diameters were coated with a thin layer of PPFEMA coating using the iCVD technique. Contact angles as high as 163° were achieved for the PPFEMA coated porous mats. The PPFEMA coated PCL and PMMA fiber mats exhibited a stable superhydrophobicity.

5.2 Introduction

The surface modification of high aspect ratio microstructures has applications in several fields such as biology, textiles, and microelectronics.^{1,2,3} For example, plasma-induced grafting has been used to attach hydrophilic polymers onto the surfaces of hydrophobic membranes in order to prevent membrane fouling caused by protein adsorption.^{4,5} Surface modification techniques allow for microporous and nanoporous structures to be fabricated using robust, inexpensive, and inert materials and subsequently functionalized to tailor surface energy or biological specificity.

iCVD is a one-step, low energy process (0.01 W/cm^2) that can be used to produce polymeric thin films in which the pendant chemical moieties are kept intact.⁶ This all-dry process has environmental benefits because no solvents are used. The iCVD process can be used to conformally coat small features such as carbon nanotube forests⁷ and particles⁸ since the surface tension problems associated with liquids are not present. The iCVD technique has been used to polymerize a wide variety of vinyl monomers such as glycidyl methacrylate⁹ and 2-hydroxyethyl methacrylate.¹⁰ The proposed polymerization mechanism is the classical free radical polymerization mechanism of vinyl monomers. Monomer and initiator gases are fed into a vacuum chamber where resistively heated wires are used to thermally decompose the initiator molecules into free radicals. Tert-butyl peroxide is commonly used as the initiator. The initiator radicals then diffuse to the substrate and adsorb onto the surface. The substrate temperature is kept cool to promote the adsorption of the free radicals as well as the monomer molecules. The initiation, propagation, and termination events occur on the surface of the cooled substrate to form a polymer film. The deposition rates achieved in the iCVD process ($\sim 200 \text{ nm/min}$) are an

order of magnitude higher than the deposition rates achieved in pulsed plasma polymerization.¹¹ The slow deposition rates in plasma polymerization are due to the complexity of the plasma process. The high energy of the plasma partially breaks the monomer and there is also a competition between etching and deposition. The iCVD process only breaks the initiator and leaves the monomer completely intact.

Low surface energy polymeric coatings have many uses due to their hydrophobic and oleophobic properties.^{12,13} For example, fluorinated polymer coatings have been used to modify various surfaces such as carbon nanotubes⁷ and textiles.^{14,15} Polymers containing CF₃ end groups have a lower surface energy (9.3 mN/m) than poly(tetrafluoroethylene) (PTFE, 18 mN/m)¹⁶ and therefore it is advantageous to create low surface energy coatings from acrylate and methacrylate monomers that contain CF₃ end groups.¹⁷ The iCVD technique has recently been used to polymerize perfluoroalkylethyl methacrylate (PFEMA) (CH₂=C(CH₃)COOCH₂CH₂(CF₂)_nCF₃ where n=5-13, n_{avg}=8) in order to create low surface energy copolymer films.¹⁸

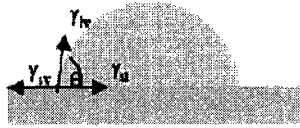
The hydrophobicity of a flat substrate can be increased either by lowering the surface energy through a change in surface chemistry or by adding roughness to the surface.^{19,20} It has been found that the maximum contact angle that can be achieved on a flat surface using surface chemistry alone is 120°²¹ and static contact angles higher than 120° can only be achieved through the addition of surface roughness. A rough, hydrophobic surface can exist in two different states: Wenzel or Cassie-Baxter. In the Wenzel state,²² the water droplet penetrates the pore and there is a large hysteresis between advancing and receding contact angles. In the Cassie-Baxter state,²³ the water droplet does not penetrate the pore and instead sits on top of the pores. There is low

hysteresis in the Cassie-Baxter state. In the Cassie-Baxter model, the apparent contact angle, θ^* , is $\cos \theta^* = \phi_s \cos \theta - \phi_v$, where θ is the contact angle on a flat surface and ϕ_s and ϕ_v are the solid-liquid and air-liquid contact area per unit projected surface area respectively. (Figure 5-1) For practical applications that require hydrophobicity, water droplets should not penetrate the pores and therefore the Cassie-Baxter state is required.

Electrospinning is a technique that uses an electric field to create polymer fibers that can have diameters as small as 100 nm.²⁴ At a critical voltage, an electrically charged jet deposits as a single, continuous fiber onto a grounded target. The fiber mat that results is nonwoven. Electrospinning can produce fibers that are two orders of magnitude smaller than those produced using conventional extrusion techniques. These small fibers can be used to make filters and membranes.²⁵

The goal of this study is to combine the iCVD method with the electrospinning method in order to create superhydrophobic mats. In the first study, beaded and non-beaded electrospun poly(caprolactone) (PCL) fiber mats will be coated with a thin layer of poly(perfluoroalkylethyl methacrylate) (PPFEMA) coating using the iCVD technique. In the second study, porous electrospun poly(methyl methacrylate) (PMMA) mats will be coated with a thin layer of PPFEMA coating using the iCVD technique. The hypothesis is that the inherent roughness of the electrospun fiber mats can be combined with the low surface energy of the PPFEMA coating in order to make superhydrophobic surfaces.

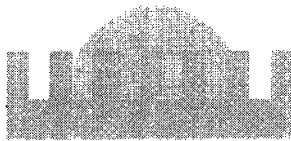
a)



Young's equation

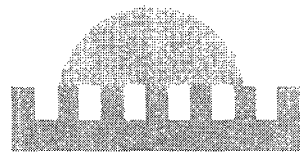
$$\cos \theta = \frac{\gamma_{sv} - \gamma_{sl}}{\gamma_{lv}}$$

b)



Wenzel
high hysteresis

c)



Cassie-Baxter
low hysteresis

$$\cos \theta^* = \phi_s \cos \theta - \phi_f$$

Figure 5-1: a) Contact angles on flat substrates can be estimated using Young's equation. Contact angles on rough surfaces can exist in one of two states b) the Wenzel state and c) the Cassie-Baxter state. In the Wenzel state, the water falls into the pores and there is high hysteresis. In the Cassie-Baxter state, the water sits on top of the pores and there is low hysteresis.

5.3 Experimental Methods

Poly(caprolactone) (PCL) (Aldrich) ($M_w=80K$) was mixed with chloroform (Aldrich) and methanol (Aldrich) and the solution was electrospun using a parallel plate setup described elsewhere.²⁶ Porous poly(methyl methacrylate) (PMMA) mats were made by electrospinning a chloroform solution in ambient conditions with 44% humidity. The iCVD polymerization was conducted in a custom-built cylindrical reactor (240 mm diameter, 33 mm height). Perfluoroalkylethyl methacrylate (PFEMA) ($CH_2=C(CH_3)COOCH_2CH_2(CF_2)_nCF_3$ where $n=5-13$, $n_{avg}=8$) monomer and tert-butyl peroxide initiator (98%, Aldrich) were used without further purification. The PFEMA monomer was heated to 90°C and fed into the chamber at a flowrate of 0.8 sccm through a heated mass flow controller (Model 1152C, MKS) and the initiator was kept at room temperature and fed into the chamber at a flowrate of 0.1 sccm through another mass flow controller (Model 1479A, MKS). The reactor pressure was kept constant at 300 mTorr. Nichrome filaments (80% Ni/20% Cr) were resistively heated to 250°C. The distance between the filaments and the substrate was kept at 29 mm. The electrospun fiber mats were placed onto a stage that was backside cooled to a constant temperature of 44°C using water from a recirculating chiller. The film thickness was measured on a reference silicon wafer using profilometry (Tencor P10).

X-ray photoelectron microscopy (XPS) (Kratos AXIS Ultra spectrometer with a monochromatized Al K α source) was used to study the chemical composition of the membranes. Contact angle measurements were conducted using a goniometer (Ramé-Hart Model 500). Scanning electron microscopy (SEM) (JEOL 6060) was used to image the electrospun mats.

5.4 Results and Discussion

5.4.1 PPFEMA-coated Beaded and Non-Beaded PCL Fiber Mats

Poly(caprolactone) (PCL) electrospun mats were used because PCL is a biodegradable polymer and therefore has many uses in biological applications.²⁷ Both beaded and non-beaded PCL electrospun mats were studied. Beaded fibers are created when the electrospinning jets break up due to the capillary action caused by surface tension.²⁸ The beading phenomenon can be controlled by varying the viscoelasticity of the solution, the charge density of the jet, and the surface tension of the solution. Both the beaded and non-beaded PCL mats were coated with a thin layer of PPFEMA coating using the iCVD process.

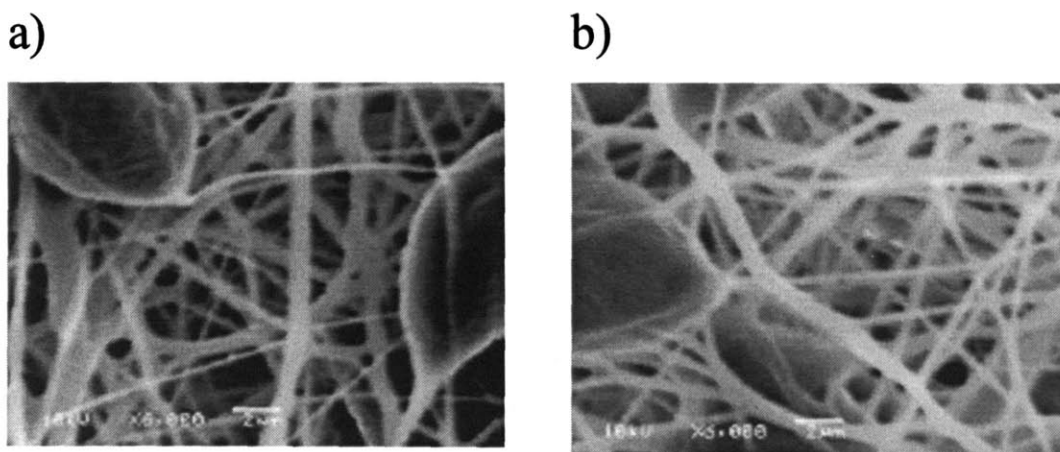


Figure 5-2: SEM micrographs of a beaded PCL electrospun fiber mat a) before and b) after coating. There is no noticeable change in the morphology of the fibers after coating.

Figure 5-2 compares the SEM micrographs of a beaded PCL electrospun fiber mat before and after coating. The PPFEMA coating thickness is 70 nm as measured on a reference silicon wafer. The actual thickness around each individual fiber is much less than 70 nm due to the high surface area of the mats. It can be seen that the thin layer of

PPFEMA coating does not change the morphology of the PCL fiber mat and therefore the inherent roughness of the electrospun mat is kept intact.

Figure 5-3 compares the XPS survey scans of a PCL electrospun fiber mat before and after coating. Since the fiber mat is made of poly(caprolactone), the spectrum of the uncoated mat contains only carbon and oxygen peaks. The spectrum of the coated mat contains fluorine peaks confirming the presence of the PPFEMA coating.

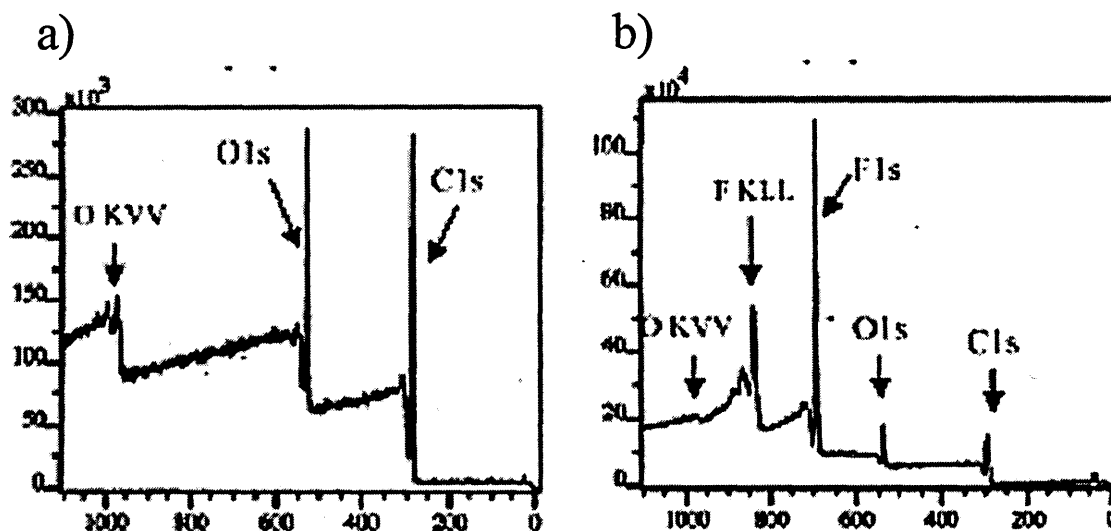


Figure 5-3: XPS survey scans of a) an uncoated PCL mat and b) a PPFEMA coated PCL mat. The spectrum of the coated mat contains fluorine peaks confirming the presence of the PPFEMA coating.

Figure 5-4a shows the water contact angles on beaded and non-beaded PCL electrospun fiber mats before coating. Although the contact angles are high and the mats appear hydrophobic, this hydrophobicity is metastable. After a few minutes, the water droplet penetrates the pores of the mat. The uncoated PCL mats are therefore in the Wenzel state. The droplet pins to the mat and does not slide off even when the mat is tilted to 90° . There are a couple of trends that can be seen from the figure: the contact

angles for both the beaded and non-beaded fibers increase as the average fiber diameter decreases and the contact angles for the beaded fibers increase as the bead density increases and the bead size decreases. These trends are caused by the fact that thinner, beaded fibers have a higher surface roughness than thicker, non-beaded fibers.

Figure 5-4b shows the water contact angles on the PPFEMA coated PCL electrospun fiber mats. The contact angles on the PPFEMA coated mats are higher than those on the uncoated mats and the trends are the same with regard to fiber diameter and bead size and bead density. A contact angle as high as 175° is achieved. More importantly the hydrophobicity on the coated mats is stable. Figure 5-5 shows the threshold sliding angles for a 20 mg water droplet on the PPFEMA coated mats. The sliding angles are all less than 12° which shows that the water droplet does not penetrate the pores of the mat and therefore does not pin to the mat. The PPFEMA coated mats therefore exist in the desirable Cassie-Baxter state. The trends in sliding angles are the same as that for contact angles: the thinner, beaded fibers have lower sliding angles than thicker, non-beaded fibers. The lowest sliding angle achieved was 2.5° which corresponds to the electrospun mat with the highest contact angle of 175° .

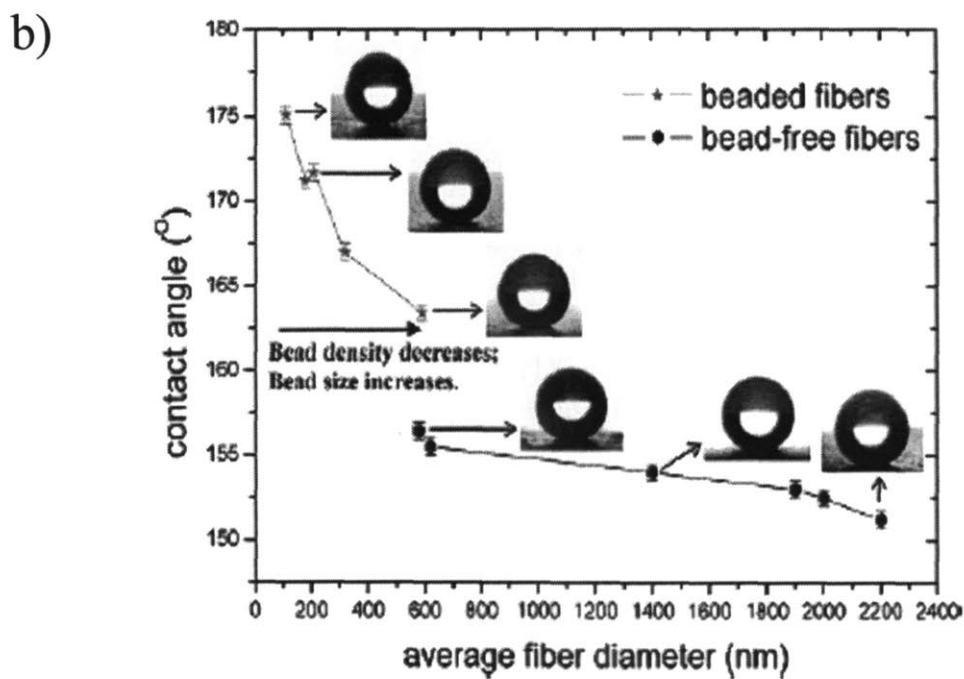
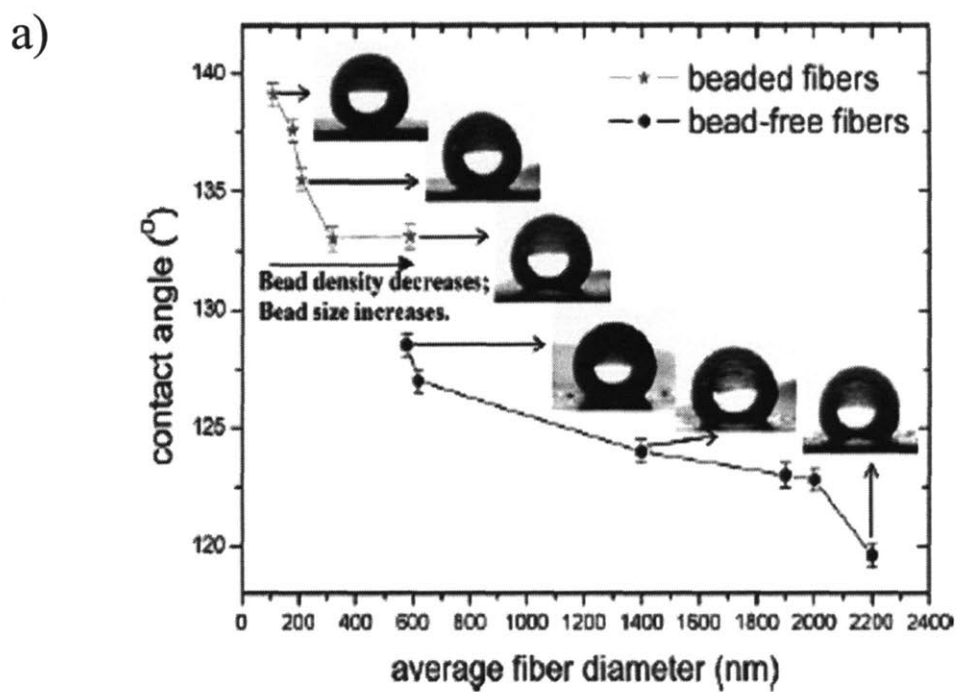


Figure 5-4: Contact angles on the PCL electrospun fiber mats a) before and b) after coating. The contact angles increase after coating.

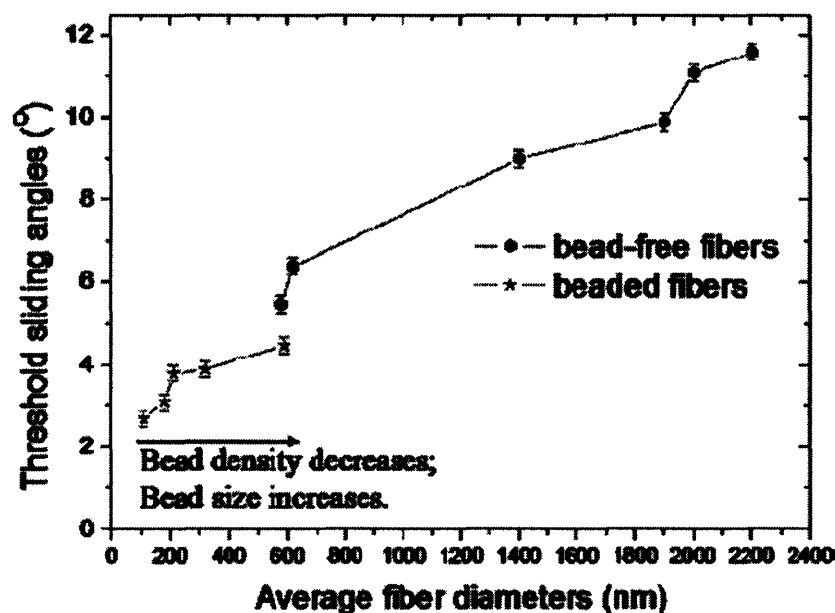


Figure 5-5: Threshold sliding contact angles on the PPFEMA coated PCL electrospun fiber mats.

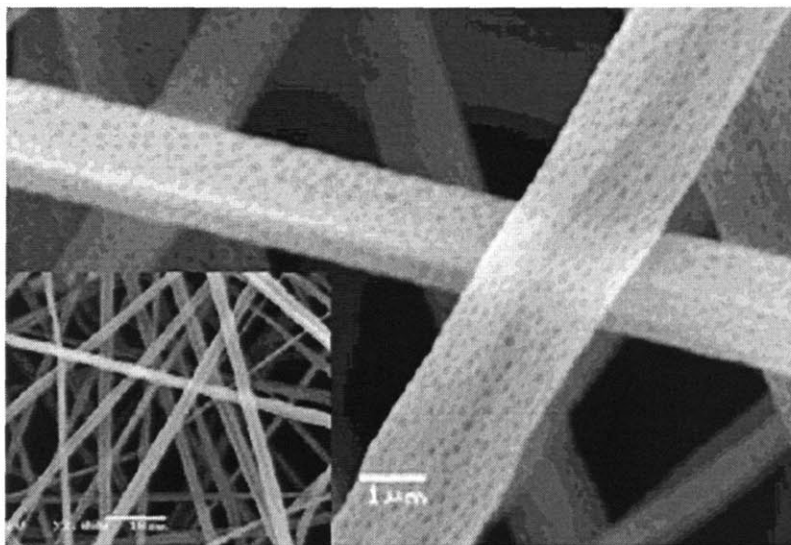
5.4.2 PPFEMA-coated PMMA Porous Fiber Mats

Electrospun poly(methyl methacrylate) (PMMA) mats with 1.7 μm fiber diameters and 80 nm pore diameters were made by electrospinning a chloroform solution in ambient conditions with 44% relative humidity. The pore structures form from the rapid phase separation and the moisture in the air. These porous PMMA mats were coated with a thin layer of PPFEMA using the iCVD technique.

Figure 5-6 compares the SEM micrographs of a porous PMMA electrospun fiber mat before and after coating. The PPFEMA coating thickness is 30 nm as measured on a reference silicon wafer. The actual thickness around each individual fiber is much less than 30 nm due to the high surface area of the mats. It can be seen that the thin layer of

PPFEMA coating does not clog the nanopores and therefore the inherent roughness of the porous electrospun mat is kept intact.

a)



b)

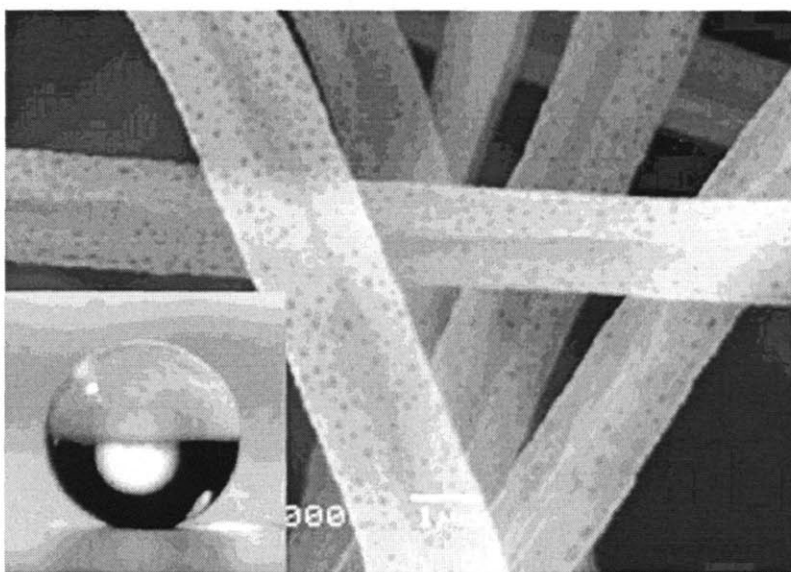


Figure 5-6: SEM micrographs of a porous PMMA electrospun mats a) before and b) after coating. There is no noticeable change in morphology after coating. The nanopores remain open even after coating.

The contact angle on the uncoated porous PMMA mat is 147° which is higher than the contact angle (144°) on a non-porous uncoated PMMA mat of the same fiber diameter ($1.7\ \mu\text{m}$). This increase in hydrophobicity is to be expected because the nanopores add another level of roughness to the electrospun mats. Although the contact angle for the uncoated porous mat is high, the hydrophobicity is metastable. After a few minutes, the contact angle decreases to 74° and therefore there is a high hysteresis. The uncoated porous PMMA mats are therefore in the Wenzel state. This is to be expected since the uncoated PCL mats were also in the Wenzel state.

After coating with PPFEMA, the contact angle on the porous PMMA mat increases to 163° . More importantly the hydrophobicity on the coated mat is stable. After a few minutes, the contact angle decreases only slightly to 160° and therefore there is very low hysteresis. The PPFEMA coated mats therefore exist in the desirable Cassie-Baxter state.

5.5 Conclusion

The initiated chemical vapor deposition (iCVD) method was combined with the electrospinning method in order to create superhydrophobic mats. The superhydrophobicity was achieved through the combination of the inherent roughness of the electrospun mats and the low surface energy of the PPFEMA coating. SEM images verified that the coating does not affect the morphology of the electrospun mats and XPS scans verified the presence of the fluorine coating. The PPFEMA coated PCL and PMMA fiber mats were found to exist in the desirable Cassie-Baxter since these coated mats exhibited a very low contact angle hysteresis. Contact angles as high as 175° and sliding angles as low as 2.5° were obtained for the PPFEMA coated PCL mats. Contact

angles as high as 163° were obtained for the PPFEMA coated PMMA mats. This work demonstrates that the iCVD method can be used to modify the surfaces of complex 3-dimensional objects such as beaded and porous electrospun mats.

5.6 Acknowledgments

We would like to thank our collaborators Minglin Ma and Professor Gregory Rutledge. This research was supported in part by the U.S. Army through the Institute for Soldier Nanotechnologies, under contract DAAD-19-02-D-0002, with the U.S. Army Research Office. The content does not necessarily reflect the position of the government, and no official endorsement should be inferred.

5.7 References

- (1) S. E. Létant, B. R. Hart, A. W. Van Buuren, L. J. Terminello, *Nat. Mater.* **2003**, *2*, 391.
- (2) R. G. Gordon, D. Hausmann, E. Kim, J. Shepard, *Chem. Vap. Deposition* **2003**, *9*, 73.
- (3) L. P. Yeo, Y. H. Yan, Y. C. Lam, M. B. Chan-Park, *Langmuir* **2006**, *22*, 10196.
- (4) D. S. Wavhal, E. R. Fisher, *Journal of Membrane Science* **2002**, *209*, 255.
- (5) H.-Y. Yu, M.-X. Hu, Z.-K. Xu, *Plasma Process. Polym.* **2005**, *2*, 627.
- (6) Y. Mao, K. K. Gleason, *Langmuir* **2006**, *22*, 1795.
- (7) K. K. S. Lau, J. Bico, K. B. K. Teo, M. Chhowalla, G. A. J. Amaratunga, W. I. Milne, G. H. McKinley, K. K. Gleason, *Nano Lett.* **2003**, *3*, 1701.
- (8) K. K. S. Lau, K. K. Gleason, *Adv. Mater.* **2006**, *18*, 1972.
- (9) Y. Mao, K. K. Gleason, *Langmuir* **2004**, *20*, 2484.
- (10) K. Chan, K. K. Gleason, *Langmuir* **2005**, *21*, 8930.
- (11) M. Gupta, K. K. Gupta, *Langmuir*, **2006**, *22*, 10047.
- (12) Feng, L.; Li, S.; Li, Y.; Li, H.; Zhang, L.; Zhai, J.; Song, Y.; Liu, B.; Jiang, L.; Zhu, D. *Adv. Mater.* **2002**, *14*, 1857-1860.
- (13) Chen, W.; Fadeev, A. Y.; Hsieh, M. C.; Oner, D.; Youngblood, J.; McCarthy, T. J. *Langmuir* **1999**, *15*, 3395-3399.
- (14) Furukawa, Y.; Kotera, M. *J. Appl. Polym. Sci.* **2003**, *87*, 1085-1091.
- (15) McCord, M. G.; Hwang, Y. J.; Qiu, Y.; Hughes, L. K.; Bourham, M. A. *J. Appl. Polym. Sci.* **2003**, *88*, 2038-2047.
- (16) Thunemann, A. F.; Lieske, A.; Paulke, B.-R. *Adv. Mater.* **1999**, *11*, 321-324.
- (17) Park, I. J.; Lee, S. B.; Choi, C. K.; Kim, K. J. *J. Colloid Interface Sci.* **1996**, *181*, 284-288.

-
- (18) Mao, Y.; Gleason, K. K. *Macromolecules* **2006**, *39*, 3895-3900.
- (19) X. Feng, L. Jiang, *Adv. Mater.* **2006**, *18*, 3063.
- (20) H. Chen, F. Zhang, S. Fu, X. Duan, *Adv. Mater.* **2006**, *18*, 3089.
- (21) A. Lafuma, D. Quere, *Nat. Mater.* **2003**, *2*, 457.
- (22) R. N. Wenzel, *Ind. Eng. Chem.* **1936**, *28*, 988.
- (23) A. B. D. Cassie, S. Baxter, *Trans. Faraday Soc.* **1944**, *40*, 546.
- (24) J.A. Matthews, G.E. Wnek, D.G. Simpson, G.L. Bowlin, *Biomacromolecules* **2002**, *3*, 232.
- (25) Y.M. Shin, M.M. Hohman, M.P. Brenner, G.C. Rutledge, *Appl. Phys. Lett.* **2001**, *78*, 1149.
- (26) Shin, Y. M.; Hohman, M. M.; Brenner, M. P.; Rutledge, G. C. *Polymer* **2001**, *42*, 9955.
- (27) K.H. Lee, H.Y. Kim, M.S. Khil, Y.M. Ra, D.R. Lee *Polymer* **1999**, *44*, 1287.
- (28) H. Fong, I. Chun, D.H. Reneker, *Polymer* **1999**, *40*, 4585.

Chaper Six:
Conclusions and Future Work

6.1 Conclusions

The iCVD technique is an all-dry, one-step polymerization process that has environmental benefits because no solvents are used. This process can be used to conformally coat complex geometries since the surface tension problems associated with liquids are not present and this process can also be used to coat temperature-sensitive objects since the substrates are backside-cooled. The work in this thesis has made three main contributions: 1) the iCVD technique was used to create water-repellant, self-cleaning fluoropolymer thin films, 2) the iCVD process was scaled-up from a small-scale reactor to a roll-to-roll reactor using dimensionless analysis, and 3) the iCVD process was used to modify the surfaces of complex structures such as polymeric capillary pore membranes and electrospun fiber mats. The main conclusions for each chapter are highlighted in the following sections.

6.1.1 Initiated Chemical Vapor Deposition of PPFDA Thin Films

The iCVD process was used to create low surface energy poly(1H,1H,2H,2H-perfluorodecyl acrylate) (PPFDA) thin films at deposition rates as high as 375 nm/min. This low surface energy polymeric coating has many uses due to its hydrophobic and oleophobic properties. For all iCVD PPFDA films, FTIR and XPS analysis showed full retention of the fluorine moieties and the static contact angle was found to be $120.8^\circ \pm 1.2^\circ$. It was found that both the deposition rate and the molecular weight increase with decreasing substrate temperature and increasing monomer partial pressure. Quartz crystal microbalance (QCM) measurements showed that these trends correlated with an increased monomer concentration at the surface. The deposition rate data and the QCM data were quantitatively analyzed to find the rate constants of the process using a

previously published model for the iCVD process involving nonfluorinated monomers. The determined values of the rate constants of the surface polymerization were found to be similar to the rate constants measured in liquid phase free radical polymerization. This kinetic data can be used to study iCVD polymerization onto more complex geometries.

6.1.2 Large Scale Initiated Chemical Vapor Deposition

The iCVD polymerization of glycidyl methacrylate (GMA) was scaled up in a custom modified roll-to-roll reactor using dimensionless analysis. The roll-to-roll process is a time-saving process that allows for the production of realistic size samples. A deposition rate as high as 85 nm/min was achieved on a large 12 inch by 12 inch area. The same trends were found in the roll-to-roll reactor as the small scale reactors. It was found that the deposition rate increases with increasing filament temperature and the deposition rate and the number-average molecular weight increase with decreasing substrate temperature. At substrate speeds between 20 mm/min and 60 mm/min, the deposition rate on the moving substrate was found to be equal to the deposition rate on the stationary substrate. This is to be expected since at these substrate speeds, the moving substrate is stationary relative to the gas flow and therefore there is no significant change in the flow profile. Since the iCVD polymerization of different vinyl monomers all use similar parameters, this scale up can be applied to the scale up of other vinyl monomers.

6.1.3 Surface Modification of High Aspect Ratio Pores

The iCVD process was used to functionalize polymeric capillary pore membranes with poly(1H,1H,2H,2H-perfluorodecyl acrylate) (PPFDA) polymer coating. The surface modification of high aspect ratio microstructures has applications in several fields such as biology, textiles, and microelectronics. It was found that the iCVD process could

functionalize pores with aspect ratios as high as 80:1. XPS survey scans confirmed the presence of the PPFDA coating on the topside and the backside of the membranes and electron microprobe analysis confirmed the presence of the coating along the pore wall. Static and dynamic contact angle measurements (low hysteresis) showed that the coated membranes exist in the Cassie-Baxter state. The ability to coat high aspect ratio trenches in silicon wafers was also demonstrated.

6.1.4 Surface Modification of Electrospun Mats

The iCVD process was combined with the electrospinning method in order to create superhydrophobic mats. XPS survey scans verified the presence of the fluorine coating and SEM images verified that the coating did not affect the inherent roughness of the electrospun mats. In the first study, beaded and non-beaded electrospun poly(caprolactone) (PCL) fiber mats were coated with a thin layer of poly(perfluoroalkylethyl methacrylate) (PPFEMA) coating using the iCVD technique. Contact angles as high as 175° and sliding angles as low as 2.5° were obtained for the PPFEMA coated mats. In the second study, porous electrospun poly(methyl methacrylate) mats were coated with a thin layer of PPFEMA coating using the iCVD technique. Contact angles as high as 163° were achieved for the PPFEMA coated porous mats. The PPFEMA coated fiber mats were found to exist in the Cassie-Baxter state.

6.2 Future Work

There are many topics that should be further explored especially with respect to using the iCVD technique to coat 3-dimensional objects since this is a fairly new area in our group. Chapter 4 showed that the breakthrough pressures of PPFDA coated membranes with pore diameters of 3 μm and 10 μm were found to be as high as 8.3 psi

and 2.2 psi respectively. For practical applications, hydrophobic membranes should have even higher breakthrough pressures. Since theory predicts that the breakthrough pressure is inversely proportional to the pore diameter, higher breakthrough pressures can be achieved by coating membranes with smaller pore diameters. Coating smaller pore diameters will also allow us to investigate if there is a maximum aspect ratio that can be coated using the iCVD technique.

Other future work with the capillary pore membranes includes using the iCVD process to functionalize the pore walls with other acrylate polymers. For instance, the pores can be coated with poly(2-hydroxyethyl methacrylate) in order to make hydrophilic membranes or the pores can be coated with poly(glycidyl methacrylate) and then further functionalized through a ring opening reaction.

The iCVD technique is a substrate-independent process because there is no bonding between the substrate and the coating. In order to create more durable coatings, it is often desirable to have a chemical bond between the coating and the substrate. Future work with the capillary pore membranes will therefore also involve creating more durable coatings by using methods such as grafting.

Chapters 4 and 5 focused on the surface modification of microstructures such as capillary pore membranes and electrospun fiber mats. These chapters show that the iCVD technique allows for microporous and nanoporous structures to be fabricated using robust, inexpensive, and inert materials and subsequently functionalized to tailor surface energy or biological specificity. Future work in this area will involve using the iCVD process to modify the surfaces of other complex geometries such as microchannels,

trenches, and nanopores for applications in several fields such as biology, textiles, and microelectronics.

Fundamental research must be done in order to fully understand the mechanism involved in the iCVD coating of complex structures. It is important to understand how different reaction conditions affect the conformality of the coating along the substrate surfaces. Some preliminary work has been done using silicon trenches (kindly provided by Dr. Edward Gleason of Analog Devices).

Silicon trenches (3 μm width, 6 μm depth, 8 μm spacing between trenches) were coated with poly(glycidyl methacrylate) (PGMA) and poly(1H,1H,2H,2H-perfluorodecyl acrylate) (PPFDA) in order to visualize the coating along the trench walls.

Two sets of experiments were conducted with PGMA coating in order to determine the factors that affect the conformality of the coating along the trench walls. In the first set of experiments, the monomer flow rate was kept constant at 3 sccm and the initiator flow rate was kept constant at 1 sccm while the reactor pressure was varied between 150 mTorr and 450 mTorr. The mean free path is inversely proportional to pressure and therefore the reactor pressure might cause differences in the conformality of the coating. In the second set of experiments, the monomer flow rate was kept constant at 3 sccm and the reactor pressure was kept constant at 370 mTorr while the initiator flow rate was varied between 1 sccm and 3 sccm. Changing the initiator flow rate while keeping the monomer flow rate constant changes the ratio of initiator to monomer. It is possible that the conformality of the coating increases as the initiator ratio increases. Silicon trenches were also coated with PPFDA in order to investigate whether the choice

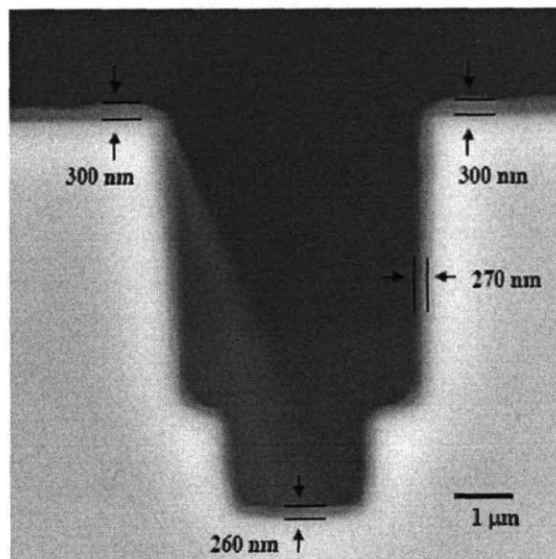
of monomer affects the conformality of the coating. Table 6-1 lists the process conditions for the PGMA and PPFDA trench coatings.

Table 6-1: Process Conditions for Trench Coatings

Sample	Coating	Substrate Temp (C°)	Filament Temp (C°)	Monomer Flow Rate (sccm)	Initiator Flow Rate (sccm)	Total Pressure (mTorr)	P_M/P_{sat}
P1	PGMA	30	280	3	1	370	0.55
P2	PGMA	30	280	3	1	450	0.67
I1	PGMA	30	280	3	1	370	0.55
I2	PGMA	30	280	3	3	370	0.37
F	PPFDA	35	300	0.6	1.3	100	0.27

Figure 6-1 shows two trenches from the pressure series. The trenches were coated at reactor pressures of 370 mTorr (sample P1) and 450 mTorr (sample P2) which correspond to P_m/P_{sat} of 0.55 and 0.67 respectively. Figure 6-2 shows two trenches from the initiator series. The trenches were coated at initiator flow rates of 1 sccm (sample I1) and 3 sccm (sample I2) which correspond to P_m/P_{sat} of 0.55 and 0.37 respectively. The PGMA coating can be visually seen along the inner trench walls. The coating is fairly uniform although there is a slight decrease in coating thickness between the top surface and the inner trench wall. The difference between the conformality of the coatings on the various trenches in the figures is currently not significant enough to make any definitive conclusion about how reactor pressure and initiator ratio affect the conformality of the coating. Figure 6-3 shows a trench coated with PPFDA (sample F). There is no noticeable difference between the conformality of the PGMA coating and the PPFDA coating and therefore monomer choice does not appear to affect coating conformality. Future work will include coating more trenches at different reaction coatings in order to further investigate which variables affect coating conformality.

a)



b)

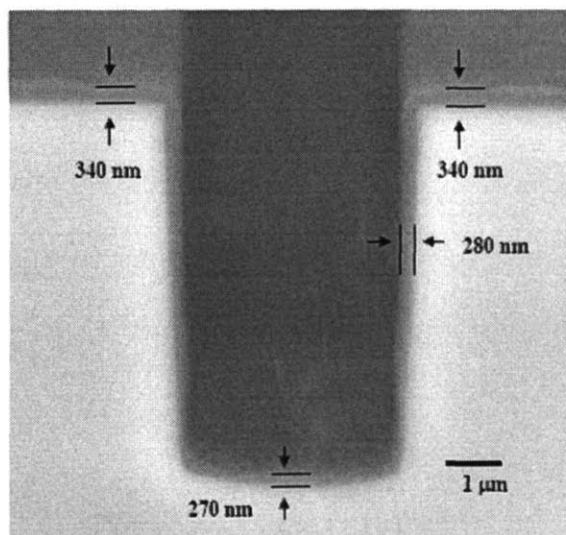
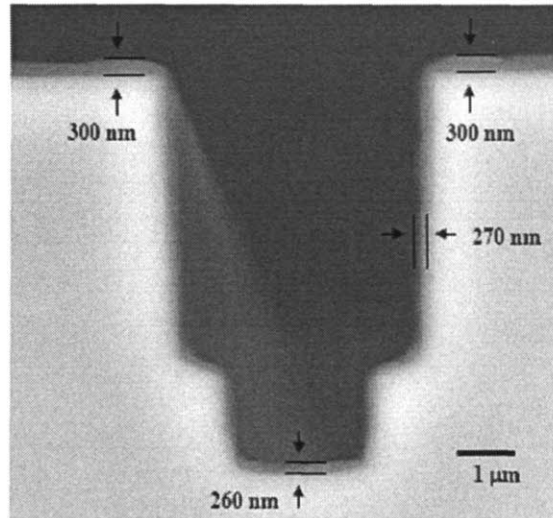


Figure 6-1: Comparison of two trenches coated with PGMA under reactor conditions in which all variables are kept the same except for the total reactor pressure. a) Trench coated at a reactor pressure of 370 mTorr (sample P1). b) Trench coated at a reactor pressure of 450 mTorr (sample P2).

a)



b)

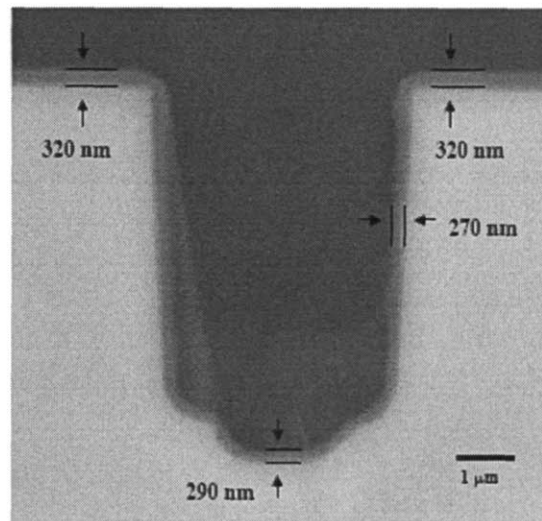


Figure 6-2: Comparison of two trenches coated with PGMA under reactor conditions in which all variables are kept the same except for the initiator flow rate. a) Trench coated at an initiator flow rate of 1 sccm (sample I1). b) Trench coated at an initiator flow rate of 3 sccm (sample I2).

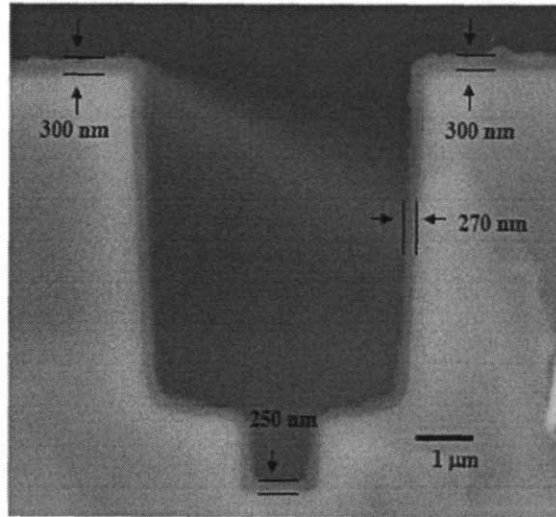


Figure 6-3: Trench coated with PPFDA (sample F).